journal

J. Am. Ceram. Soc., 73 [2] 187-206 (1990)

Perspective on the Development of High-Toughness Ceramics

Anthony G. Evans*

Materials Department, College of Engineering, University of California, Santa Barbara, California 93106

I. Major Developments

(1) Synopsis

THE science governing the strength and fracture of structural ceramics has developed from a mostly empirical topic in 1965 into a mature discipline that now sets the standards in the field of mechanical behavior. The intent of this review is to provide a perspective regarding this evolution, followed by succinct descriptions of current understanding. The rapid developments in the field are considered to have commenced upon the first concerted attempt to apply fracture mechanics concepts to ceramics, beginning in the middle 1960s (Fig. 1). This allowed a distinction between the separate contributions to strength from the flaws in the material and from the microstructure, as manifest in the fracture toughness. Another contribution that accelerated the learning process was the development of indentation techniques, which allowed trends in the damage resistance of new ceramics to be assessed on a routine basis. However, the most important development, which originated at about the same time, was the discovery of toughened zirconia alloys. The ensuing research on these alloys established two vital precedents. Firstly, the introduction of the materials-by-design approach, which established the benefits that accrue from the strong collaboration between processing, characterization, testing, and modeling (Fig. 2). Secondly, the topic attracted the attention of outstanding scientists who have since continued to provide invaluable contributions to progress in the field. Still another important development was the appreciation that the mechanical properties of ceramics could be appreciably enhanced by the incorporation of ceramic fibers and whiskers. Finally, a recent discovery that may have a similar substantive impact on the ceramics field concerns metal-toughened ceramics and composites formed by directed metal oxidation.

(2) Introduction of Fracture Mechanics

The mathematical framework and the experimental techniques of linear elastic fracture mechanics that had developed from the early 1950s and had been extensively applied to metals were first recognized to have importance to the ceramic field by Davidge and by Wiederhorn. These authors examined a variety of experimental approaches and began the process whereby the fracture toughness could be established as a material parameter and eventually be related to microstructure. At the same time, initial attempts were made to separate the contributions to strength, S, from the flaw size, a, and the toughness, K_{IC}, through the simple application of the Griffith relation

$$S = YK_{IC} / \sqrt{a} \qquad (1)$$

where Y is a well-documented crack/specimen geometry parameter. Although it took some time to rigorously accomplish this objective, the first attempts brought attention to the concept of a "microstructural flaw" and soon provided a focus for processing activities concerned with the elimination of the largest flaws. This development also addressed a paradox in the field, wherein strength measurements were then typically expressed in terms of

A. H. Heuer—contributing editor

Manuscript No. 197905. Received November 20, 1989; approved December 13, 1989.

Presented in part at the 91st Annual Meeting of the American Ceramic Society, Indianapolis, IN, April 24, 1989 (Orton Memorial Lecture).

[Key words: toughness, fracture, microcracking, zirconia, R curve.]

*Member, American Ceramic Society

review

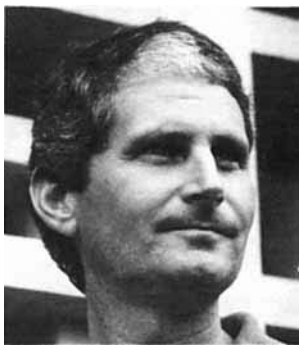

Anthony G. Evans is Alcoa Professor and Chair of the Materials Department at the Unviersity of California at Santa Barbara. A native of Wales, he earned his B.S. in metallurgy in 1964 and Ph.D. in physical metallurgy in 1967, both from Imperial College, London, England. During 1967 to 1971 he was with the Atomic Energy Research Establishment, Harwell. In 1971 Evans came to the United States as visiting scholar at the University of California at Los Angeles. He then worked at the National Bureau of Standards from 1972 to 1974, Rockwell International Science Center from 1974 to 1978, and the University of California at Berkeley from 1978 to 1985. He has more than 200 technical papers to his credit.

A Fellow of the American Ceramic Society, Evans is a past chair of the Basic Science Division and a past vice president of the Society. He received the Society's Ross Coffin Purdy Award in 1980, and was recipient of the Fulrath Award in 1981. Evans delivered the Edward Orton, Jr., Memorial Lecture and received the John Jeppson Medal and Award during the 1989 Annual Meeting of the Society. He is a member of the National Institue of Ceramic Engineers.

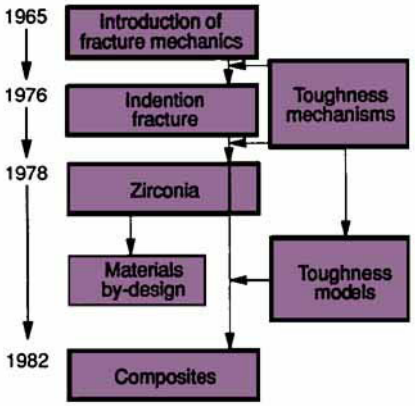

Fig. 1. Overall chronological trends in the development of high-toughness ceramics.

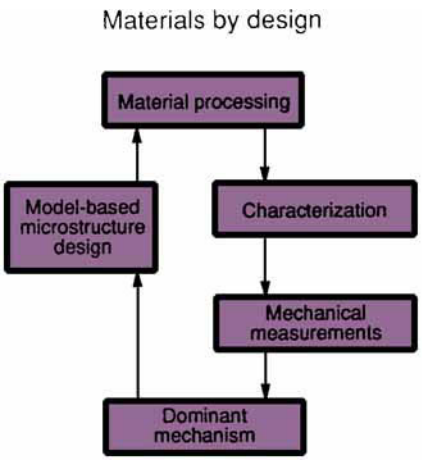

Fig. 2. Scheme involved in the materials-by-design concept.

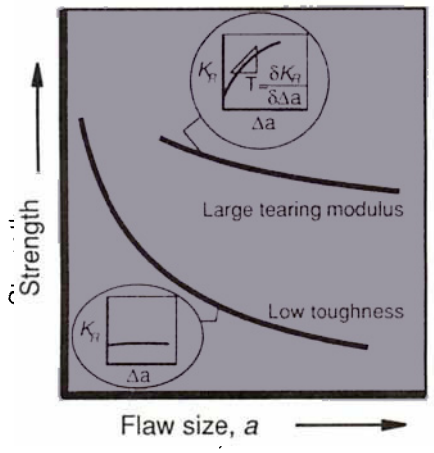

Fig. 3. Effects of damage on the strength of low- and high-toughness ceramics. The tearing modulus is the slope of the resistance curve.

average microstructural features, such as grain size and porosity, whereas differences in strength between test methods (e.g., bending and tension) were rationalized on the basis of *weakest link* statistics.

Some of the first observations concerning the interactions of cracks with the microstructure were made within the next several years. Out of these observations came preliminary concepts for fracture resistance mechanisms and the models that emerged later. Many of these concepts can be traced to the work of Lange and of R. Rice. Also, work at Harwell Laboratories in the United Kingdom established that very high toughness ceramics could be made by incorporating carbon fibers. This body of work provided a strong motivation to maintain a high level of activity in the field and to seek a better understanding of mechanisms and approaches for enhancing the reliability and damage tolerance of ceramics.

Although these prospects were evident, progress was slow for two reasons. Firstly, different methods for measuring fracture toughness often gave different results, leading to enquiries about the utility of the fracture toughness as a material parameter. Secondly, the most acceptable test methods required moderately large test specimens, whereupon the data emerged slowly and were confined to the relatively few ceramics amenable to the fabrication of sufficiently large specimens. One consequence of these factors was that the focus of much of the research in the field was on the characterization and implications of slow crack growth, with minimal attention given to the enhancement of toughness.

The first of the above issues would later be resolved upon the revelation that many polycrystalline ceramics exhibit resistance-curve behavior, as elaborated in Section I (5). However, it is interesting to note that the resistance-curve effects were first observed in 1974, but the significance was not appreciated. The second issue was addressed upon the introduction of indentation methods discussed in the following section.

(3) Influence of Indentation Fracture

The introduction of approaches for fracture toughness estimation by using various indentation methods allowed tests on small specimens and, thus, permitted rapid probing of the "damage tolerance" of many different ceramics. These approaches emerged from systematic pioneering research by Lawn over more than a decade. Of particular importance was the discovery that the cracks around hardness indentations formed on unloading and, hence, were dominated by residual fields. Appreciation of this factor permitted the identification of the nondimensional parameters that related toughness to either the size of the cracks or the failure stress after indentation.

A more recent benefit of indentation fracture has been its contribution to our understanding of the role of "toughness" in damage tolerance. Specifically, the tougher materials exhibit strengths after indentation that vary less rapidly with indentation load (crack size) than for brittle ceramics (Fig. 3). This behavior reflects the existence of a resistance curve. Indeed, this measure of toughness is probably the most useful in terms of the practical application and durability of ceramics.

Many of the indentation methods are only approximate and do not provide the quality of fracture resistance data needed to rigorously relate toughness to microstructure. The surface flaw methods, introduced first by Petrovic and Jacobson, seem to be the most precise, provided that residual stresses are eliminated by polishing out the plastic zone. However, none of these methods can be used for the highest toughness materials now available.

(4) Pivotal Role of Zirconia

The discovery in 1976 that zirconia can exhibit high toughness initiated a remarkable decade of development, culminating in materials having toughness on the order of 20 MPa·m$^{1/2}$. A sequence of material inventions in Australia, Germany, and the United States involving Garvie, Claussen, Lange, and Gupta provided the incentive. Such materials elicited outstanding characterization research by Heuer, Rühle, and Hannink and some novel experiments originating with Swain and Marshall. The results were then rationalized through a clear understanding of the responsible mechanisms, established by the micromechanics models of McMeeking, Budiansky, Hutchinson, Evans, and Marshall. This process occurred in an iterative manner built around the understanding that the process-zone size was important and that resistance-curve effects are inherent to the mechanism.

(5) Importance of Resistance Curves

All "tough" ceramics exhibit resistance curves. However, this feature of their behavior did not become apparent until about 1980. The existence of resistance-curve behavior was predicted by McMeeking and Evans to be an essential feature of transformation toughening and soon verified experimentally by Swain. These predictions placed emphasis on the transformation wake. The more general importance of the wake was demonstrated by some clever experiments conducted by Steinbrecht, who revealed that the toughness of Al_2O_3 is diminished upon removing the wake by sawing. Continued research on this topic revealed that microcrack toughening exhibits wake effects and that crack bridging by intact grain is a common feature of crack extension in polycrystals and is also an important contribution to the fracture resistance. Finally, and most recent-

ly, it has been demonstrated that toughening by fibers, whiskers, and metal networks all exhibit wake-dominated resistance-curve characteristics.

When rigorously measured and interpreted, resistance-curve behavior rationalizes effects of specimen geometry on toughness, crack-size effects, and trends in strength. Additionally, in the highest toughness materials, linear elastic behavior is violated for many of the common test specimens. Consequently, nonlinear approaches are needed to characterize material behavior.

(6) Discovery of Composites

High-work-of-fracture-fiber-reinforced ceramics consisting of carbon fiber, reinforced glasses, and glass-ceramics were first demonstrated in 1972, accompanied by the first complete model of composite behavior. However, activities on ceramic composites were not pursued vigorously until 1983, when Prewo and Brennan announced a Nicalon† SiC-fiber-reinforced glass-ceramic composite. This announcement established the possibility that ceramic composites having high resistance at elevated temperature might be possible. A major activity on ceramic-matrix composites has ensued and is still in progress. Another related discovery was that Al_2O_3 could be toughened by SiC whiskers. Together, these materials have provided the basis for the concepts of toughening by brittle reinforcements, involving the debonding and sliding properties of the reinforcement/matrix interfaces.

(7) Bibliography

Actual references to the work alluded to above can be located in Section II, which covers the various mechanisms in some detail. The reader is also referred to the seven-volume series Fracture Mechanics of Ceramics, edited by Bradt, Evans, Hasselman, and Lange (Plenum Press, New York, 1974–1983), which contains much of the chronology, plus the following basic references:

A. G. Evans and A. H. Heuer, "REVIEW—Transformation Toughening in Ceramics: Martensitic Transformations in Crack-Tip Stress Fields," *J. Am. Ceram. Soc.*, **63** [5–6] 241–48 (1980).

R. C. Garvie, R. H. J. Hannink, and R. T. Pascoe, "Ceramic Steel?," *Nature (London)*, **258**, 703–704 (1975).

A. H. Heuer, "Transformation Toughening in ZrO_2-Containing Ceramics," *J. Am. Ceram. Soc.*, **70** [10] 689–98 (1987).

A. H. Heuer, F. F. Lange, M. V. Swain, and A. G. Evans (eds.), "Transformation Toughening," *J. Am. Ceram. Soc.*, **69** [3] 169–298 (1986); *ibid.*, **69** [7] 511–84 (1986).

J. W. Hutchinson, Harvard University Report No. 58 (1974).

F. F. Lange, "Processing-Related Fracture Origins; I, Observations in Sintered and Isostatically Hot-Pressed Al_2O_3 Composites," *J. Am. Ceram. Soc.*, **66** [6] 396–98 (1983); F. F. Lange and M. Metcalf, "Processing-Related Fracture Origins: II, Agglomerate Motion and Cracklike Internal Surfaces Caused by Differential Sintering," *ibid.*, 398–406; and F. F. Lange, B. I. Davis, and I. A. Aksay, "Processing-Related Fracture Origins: III, Differential Sintering of ZrO_2 Agglomerates in Al_2O_3/ZrO_2 Composite," *ibid.*, 407–408.

J. R. Rice; p. 191 in Fracture, Vol. II, Mathematical Fundamentals. Edited by H. Liebowitz. Academic Press, New York, 1968.

R. W. Rice, "Mechanisms of Toughening in Ceramic Matrix Composites," *Ceram. Eng. Sci. Proc.*, **2** [7–8] 661–701 (1981).

R. W. Steinbrech and A. H. Heuer, "R-Curve Behavior and the Mechanical Properties of Transformation-Toughened ZrO_2-Containing Ceramics," *Mater. Res. Soc. Symp. Proc.*, **60**, 469–81 (1986).

M. V. Swain, "Inelastic Deformation of Mg-PSZ and Its Significance for Strength–Toughness Relationships of Zirconia-Toughened Ceramics," *Acta Metall.*, **33**, 2083–91 (1985).

A. V. Virkar and R. L. K. Matsumoto, "Ferroelastic Domain Switching as a Toughening Mechanism in Tetragonal Zirconia," *J. Am. Ceram. Soc.*, **69** [10] C-224–C-226 (1986).

II. Toughening Mechanisms

(1) General Features

The objective of research concerned with structural ceramics is the generation of materials having high reliability. To achieve this objective, there are two fundamentally different approaches (Fig. 4): flaw control and toughening. The *flaw control* approach accepts the brittleness of the material and attempts to control the large extreme of processing flaws. The *toughening* approach attempts to create microstructures that impart sufficient fracture resistance (Fig. 5) that the strength becomes insensitive to the size of flaws (Fig. 3). The former has been the subject of considerable research that identifies the most detrimental processing flaws, as well as the processing step responsible for those flaws.[1-3] The latter has emerged more recently, and has the obvious advantage that appreciable processing and postprocessing damage can be tolerated without compromising the structural reliability.[4,5]

The resistance of brittle solids to the propagation of cracks can be strongly influenced by microstructure and by the use of various reinforcements. The intent of the present paper is to provide a succinct review of the known effects of microstructure and of reinforcements on fracture resistance. In most cases, toughening results in resistance-curve characteristics (Fig. 5), wherein the fracture resistance systematically increases with crack exten-

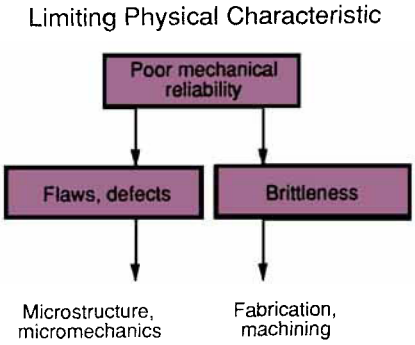

Fig. 4. Aspects for achieving high-reliability ceramics.

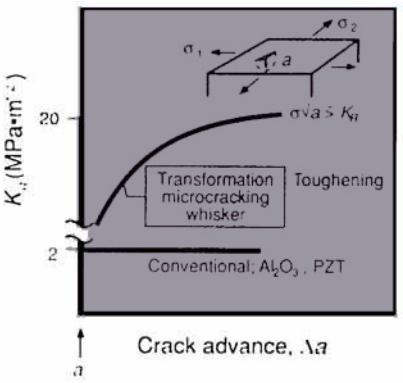

Fig. 5. Resistance-curve behavior characteristically encountered in tough ceramics: K_R is the fracture resistance and Δa is the crack advance.

†Nippon Carbon Co., Tokyo, Japan.

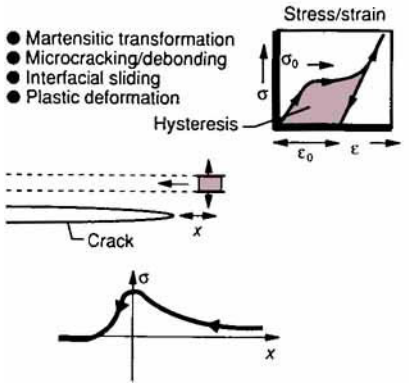

Fig. 6. Schematic diagram illustrating nonlinear hysteretic elemental response and associations with enhanced toughness.

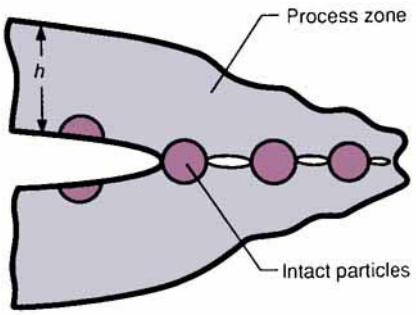

Fig. 7. Schematic diagram illustrating both process-zone and bridging-zone mechanisms of toughening.

sion. The resulting material strengths then depend on the details of the resistance curve and the initial crack lengths,[6,7] such that toughness and strength optimization usually involve different choices of microstructure. The individual mechanisms include transformations, microcracking, twinning, ductile reinforcements, fiber/whisker reinforcements, and grain bridging.

An underlying principle concerns the essential role of nonlinearity, as manifest in mechanisms of dissipation and energy storage in the material, upon crack propagation. Consequently, the potent toughening mechanisms can be modeled in terms of stress/displacement constitutive laws for representative volume elements (Fig. 6). Furthermore, the toughening can be explicitly related to stress/displacement hysteresis (Fig. 6), as will be elaborated for each of the important mechanisms. The general philosophy thus adopts the *concept of homogenizing* the properties of the material around the crack and then formulating a *constitutive law* that characterizes the three-dimensional material response. Models that discretize microstructure details in two dimensions are typically less rigorous, because three-dimensional interactions along the crack front are not readily described, and because multiple calculations are needed to eliminate artifacts of the discretization. The homogenization approach rigorously describes the toughening behavior whenever the length of the nonlinear zone is appreciably larger than the spacing between the relevant microstructural entities. *Such conditions invariably exist when the material exhibits high toughness.* The coupling between experiment and theory is another prevalent theme, because toughening is sufficiently complex and involves a sufficiently large number of independent variables that microstructure optimization only becomes practical when each of the important modes has been described by a rigorous model, validated by experiment (Fig. 2).

The known mechanisms can be conveniently considered to involve either a *process zone* or a *bridging zone* (Fig. 7). The former category exhibits a toughening fundamentally governed by a critical stress for the onset of nonlinearity, σ_{ij}^c, in elements near the crack and by the associated stress-free strain, ε_{ij}^T.[8-11] The resulting stress–strain hysteresis of those elements within a *process zone* then yields a steady-state toughness given by[11]

$$\Delta\mathcal{G}_c \approx 2f\sigma_{ij}^c \varepsilon_{ij}^T h \qquad (2)$$

where $\Delta\mathcal{G}_c$ is the increase in the critical strain energy release rate when the crack is long,‡ f the volume fraction of the toughening agent, and h the width of the process zone in steady state.[9,12] Transformation, microcrack, and twin toughening are mechanisms of this type.

The bridging category exhibits toughening governed by hysteresis along the crack surface,[13,14] induced by intact material ligaments

$$\Delta\mathcal{G}_c = 2f\int_0^{u^*} t(u)\,du \qquad (3)$$

where $2u$ is the crack opening, $2u^*$ the opening at the edge of the bridging zone, t the tractions on the crack surfaces exerted by the intact toughening agent (Fig. 7), and f the area fraction of reinforcements along the crack plane. Ductile reinforcements, as well as whiskers, fibers, and large grains, toughen by means of bridging tractions.

It is also possible for a process-zone mechanism and a bridging mechanism to operate simultaneously, and thus generate a net toughness larger than that for the separate mechanisms. Indeed, the overall toughness can even be multiplicative.[15] The operation of multiple mechanisms is probably common and needs to be addressed for each material system when toughness optimization is contemplated. Furthermore, some of the more controversial debates on mechanisms probably reflect the occurrence of multiple mechanisms, wherein the dominant mechanism changes as the microstructure is systematically varied. A particular example concerns the respective roles of grain bridging and of a microcrack process zone in various tough ceramic polycrystals.

In the "toughest" materials, a steady-

‡Short cracks and cracks without fully developed process zones give smaller changes in toughness, as elaborated in the discussion of resistance curves.

Table I. Tough Ceramics

Mechanism	Highest toughness ($MPa \cdot m^{1/2}$)	Exemplary materials	Limitation
Transformation	~20	ZrO_2 (MgO) HfO_2	$T \lesssim 900$ K
Microcracking	~10	Al_2O_3/ZrO_2 Si_3N_4/SiC SiC/TiB_2	$T \lesssim 1300$ K Strength
Metal dispersion	~25	Al_2O_3/Al ZrB_2/Zr Al_2O_3/Ni WC/Co	$T \lesssim 1300$ K Oxidation
Whiskers/platelets	~15	Si_3N_4/SiC Si_3N_4/Si_3N_4 Al_2O_3/SiC	Oxidation $T < 1500$ K
Fibers	≥30	CAS*/SiC LAS†/SiC Al_2O_3/SiC SiC/SiC SiC/C Al_2O_3/Al_2O_3	Processing Coatings Fibers

*Calcium aluminum silicate glass-ceramic. †Lithium aluminum silicate glass-ceramic.

state cracking phenomenon occurs,[16-19] wherein the crack extension stress becomes *independent of crack length.* For such materials, the toughness is usually nonunique and not, therefore, a useful design parameter. Instead, the steady-state cracking stress and the ultimate strength become the more relevant material properties. *Transitions between toughness control and steady-state cracking are thus of major significance.*

Some of the materials to be considered in this review are summarized in Table I. This list is impressive when it is appreciated that conventional ceramics have a toughness, K_c, of ≈1 to 3 MPa·m$^{1/2}$. However, some caution is also necessary because the highest levels of toughness cannot usually be used to effectively enhance strength and reliability.

(2) Process Zone Mechanisms

An important basic feature of process-zone mechanisms concerns the contribution to toughening that derives from each layer, dy, a distance y from the crack plane (Fig. 8). These contributions are, in turn, governed by specific aspects of the stress-strain curve. An issue of fundamental importance concerns the material behavior at large strains. Notably, if the material remains nonlinear beyond the critical transformation strain, the steady-state energy dissipation density caused by the nonlinearity increases as y diminishes and tends to infinity as $y \to 0$, because the strain at the crack front is infinite. Consequently, it has been appreciated for a long time that the energy release rate at the crack tip *in steady-state is strictly zero.* In this case, $\Delta\mathcal{G}_c$ can only be calculated by having *detailed knowledge* of the dimensions of the zone in which the crack-tip fracture mechanism occurs. This difficulty has prevented rigorous modeling of the contribution to the toughness of metals provided by plastic dissipation within a plastic zone. The same problem does not exist when the nonlinear deformation process saturates, such that the stress–strain curves become linear at large strain, as illustrated in Fig. 6. In this case, both $\mathcal{G}$ and K have *finite values* at the crack tip ($\mathcal{G}_{tip}$ and K_{tip}, respectively), because the material around the tip is now linear and there is no steady-state dissipation in this saturation zone. Consequently, a crack-growth condition can be identified wherein either $\mathcal{G}_{tip}$ or K_{tip} may be equated to a critical value, governed by the nature of the material immediately ahead of the crack tip. This saturation approach has been adopted for toughening mechanisms in ceramics, largely motivated by the transformation-toughening problem wherein a saturation condition can be *rigorously identified* (see Fig. 9), based on the transformation strain. However, the incidence of saturation is less apparent for other mechanisms.

Another interesting feature of process-zone problems concerns the role of the modulus of the material in the saturation region (Fig. 6). When the saturation modulus differs from the initial modulus of the material, as in microcrack toughening, the magnitude of the stress intensity at the tip, K_{tip}, is dominated by the saturation modulus, because the crack tip is essentially embedded in material having this modulus. Furthermore, the modulus effect is independent of the size of the process zone, because linearity exists near the crack tip. Consequently, accurate knowledge of the material behavior within the saturation zone, when present, is needed to adequately simulate crack-extension behavior.

A final issue, when either K_{tip} or $\mathcal{G}_{tip}$ is used as a fracture criterion, concerns the choice of the critical value of these quantities. Specifically, it is evident that the crack extends into material modified by the mechanism that occurs in the process zone. However, it is often difficult to independently ascertain the fracture resistance of material in this state.

(A) Transformation Toughening

(i) Basic Features

The stress-induced transformations that can cause significant toughening include martensitic and ferroelastic transformations, as well as twinning. The former involve both dilatational and shear components of the transformation strain, while the later typically has only a shear component. At the simplest level, transformation toughening can be regarded as a process dominated by a volume increase (dilatational stress-free strain, ε_{ii}^T). Then, based on simple concepts elaborated below, it is apparent that a stress-induced frontal process zone must have no effect on the crack-tip field, and, thus, initial crack growth must occur without toughening (Fig. 10).[9,10] However, upon crack extension, process-zone elements unload in the wake, hysteresis occurs (Fig. 9), and toughening develops, as given by

$$\Delta\mathcal{G}_c = 2f\bar{\sigma}^c h\varepsilon_{ii}^T \qquad (4)$$

where $\bar{\sigma}^c$ is the critical mean stress for supercritical§ transformation. This steady-state level of toughening is attained after substantial crack extension. A directly equivalent result for the increase in critical stress intensity factor, ΔK_c, can be derived by appreciating that a residual compressive stress is created within the transformation zone. This stress inhibits crack opening, resulting in crack shielding, such that

$$\Delta K_c = 0.22E\varepsilon_{ii}^T f\sqrt{h}/(1-\nu) \qquad (5)$$

where E is the composite modulus and ν is Poisson's ratio.

A comparison of the predicted values with experimental data based on *actual*

§Supercritical refers to the condition wherein *all* particles within the process zone *fully* transform.

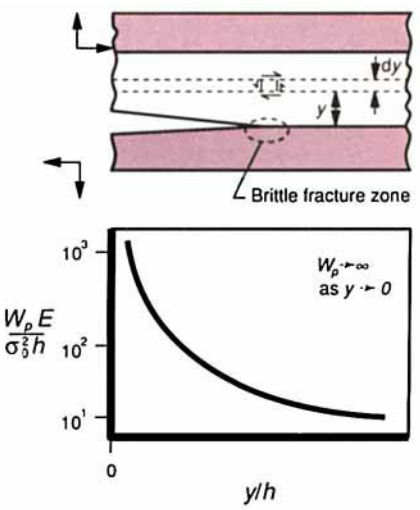

Fig. 8. Effects of distance on the dissipation that occurs in each layer of the process zone.

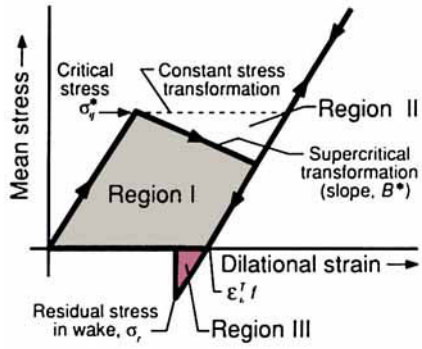

Fig. 9. Schematic stress–strain curve for the supercritical martensitic transformation indicating the critical stress and the permanent strain.

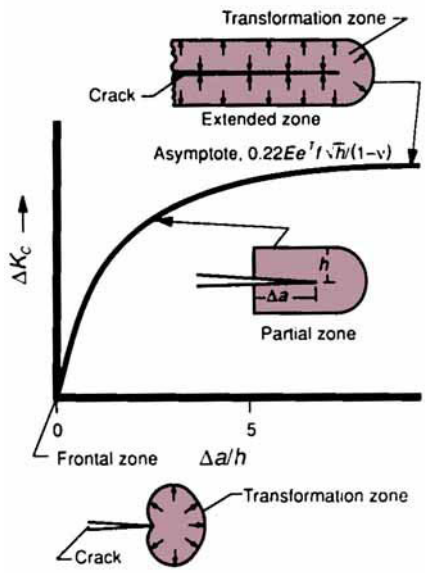

Fig. 10. Transformation zones illustrating the dimensions used in describing the transformation-toughening process: a frontal zone and a steady-state zone for a dilatational driven transformation.

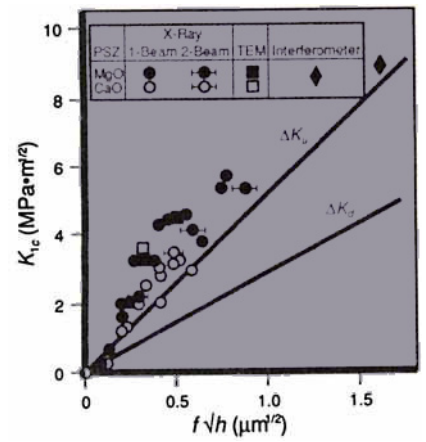

Fig. 11. Comparison between theory and experiment for various partially stabilized zirconia materials: ΔK_u refers to a zone shape dictated by the equivalent stress, whereas ΔK_σ refers to a zone shape governed by the mean stress.

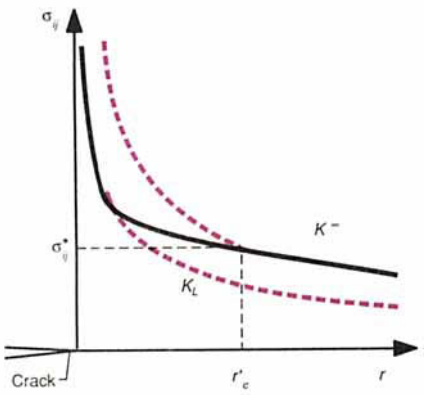

Fig. 12. Crack-tip stress fields in the presence of a dilatational transformation zone for a supercritical transformation.

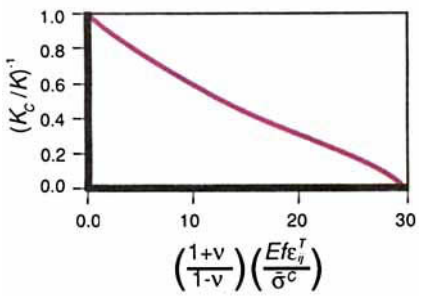

Fig. 13. Change in normalized toughness as a function of normalized transformation strain.

zone sizes measured in steady state[20] (Fig. 11) has revealed that Eq. (5) predicts the correct trends but consistently underestimates the toughness by a factor of ≈2. It has been surmised that the disparity arises because shear effects have not been incorporated. One hypothesis regarding the shear strain involves nonassociated flow.[8] Specifically, it is presumed that the *shear stress dominates the nucleation* of the transformation, but that the *residual strain is predominantly dilatational*, because of extensive twinning.[21] This premise results in a zone profile, in plane strain, with diminished transformed material ahead of the crack. The resultant toughening exceeds Eq. (5) and, furthermore, agrees quite well with experimental data (Fig. 11). However, the necessary zone shapes are not consistent with those observed by experiment.[22] Some inconsistency thus remains to be addressed, and other shear postulates, as well as the operation of additional mechanisms, such as twin-induced microcracking (see Section II(2)), may be involved.

The zone size, h, represents the major *microstructural influence on toughness*. Clearly, h is governed by a martensite nucleation law. However, a fully validated law does not yet exist. Consequently, connections between h and the microstructure still cannot be specified. Nevertheless, certain trends are apparent, based on the free energy of the fully transformed product. *Specifically, h invariably decreases* with increase in temperature and decrease in particle size. *A temperature- and particle-size-dependent toughness is thus inevitable for this mechanism.*

(ii) Constitutive Laws

Constitutive laws expressly relate the components of the stress and transformation strain tensors in the transforming solid. The stresses are most conveniently expressed in terms of the mean stress, $\bar{\sigma}$, the deviatoric stresses, $s_{ij} = \sigma_{ij} - \delta_{ij}\bar{\sigma}$, and/or the equivalent stress, $\sigma_e = \sqrt{3 s_{ij} s_{ij}/2}$, and their variation during transformation. Such relations are, in fact, the equivalent of the more familiar constitutive laws used to describe plastic deformation and crack-tip fields in elastic/plastic solids. A viable constitutive law must account for the effect of particle size and shape upon the incident of transformation by allowing only a certain fraction, f, of the solid to actually transform at a given imposed stress, σ_{ij}. The simplest yield criterion has the form[23]

$$\frac{\bar{\sigma}}{\Omega} + \frac{\sigma_e}{\tau} = 1 \tag{6}$$

where Ω and τ are experimentally determined, normalizing parameters that depend on f, ε^T_{ij}, and particle size. Experiments performed on partially stabilized zirconia (PSZ) and tetragonal zirconia polycrystals (TZP) are consistent with this transformation condition.[23] However, knowledge of the nucleation is not yet sufficient to allow Ω and τ to be expressed explicitly in terms of these variables.

(iii) Crack-Tip Stress Fields

The general form of the crack-tip stress field in the presence of a transformation zone, depicted in Fig. 12, is characterized by two stress intensity factors.[9] Outside the zone, for small-scale transformation (i.e., a small zone compared with crack length and specimen dimensions), the field is given by the linear elastic solutions ($h<r\leq a$)

$$\sigma_{ij} = (K_\infty/\sqrt{2\pi r})\,\tilde{\sigma}_{ij} \tag{7}$$

where K_∞ is the stress intensity determined by the applied loads and r the distance from the crack tip. Close to the tip, the transformation strain is saturated, and, hence, the material is again linear and can, consequently, be characterized by another stress intensity factor, K_{tip}, such that

$$\sigma_{ij} = (K_{tip}/\sqrt{2\pi r})\,\tilde{\sigma}_{ij} \tag{8}$$

The coefficient $\tilde{\sigma}_{ij}$, which depends on the polar angle, approaches that for elastic materials when $f\varepsilon^T_{ij}E/o^c_{ij}$ is small.

The transformation may thus be characterized by a stress intensity change, ΔK, defined as

$$\Delta K = K_{tip} - K_\infty \tag{9}$$

When $K_{tip}<K_\infty$, *the transformation zone shields the tip from the applied loads.* The fracture behavior is governed by the values of K_{tip} and K_∞ at the fracture criticality. Knowledge of the stress in the intervening regions is not required for analysis of the toughening.[10] Specifically, the near-tip field provides a plausible crack-extension criterion

$$K_{tip} = K_0 \tag{10}$$

where K_0 is the fracture *resistance* of the material in the transformation zone immediately ahead of the crack tip, whereupon, the *observed toughness* is

$$K_c = K_0 + \Delta K_c \tag{11}$$

where ΔK_c is the quantity $-\Delta K$, evaluated at the fracture criticality.

(iv) Toughening and Resistance Curves

There are two equivalent analytical methods for determining trends in toughness: one based on stress intensity factors, ΔK, and the other on conservation integrals $\Delta\mathcal{J}$. Both approaches predict the same behavior, but have different utility when various aspects of toughening require elucidation. Consequently, both approaches are briefly described. The approach based on *stress intensity factors* indicates that the magnitude of ΔK clearly depends on the shape of the zone and on the components of the transformation strain tensor. Initially, it is pertinent to consider a crack in an untransformed parent, such that a *frontal zone* develops as the

load is imposed. Subsequently, a *steady-state zone* of uniform width over the crack surfaces (Fig. 10) is examined. The ΔK levels are different for these two zone configurations, resulting in *R*-curve effects.[9]

For the stationary crack, when the long range strain field of the transformed particles is purely dilatational,¶ the mean stress dictates the shape of the transformation zone, which then has the shape depicted in Fig. 10. For this condition, $\Delta K = 0$. For the *steady-state* configuration and when the transformation does not reverse in the wake, as well as when all particles within h are transformed, the plane strain zone width for *small-scale* dilatational transformation is[9,10]

$$h = \frac{\sqrt{3}\,(1+\nu)^2}{12\pi}\left(\frac{K_\infty}{\bar{\sigma}^c}\right)^2 \qquad (12)$$

The corresponding extent of crack shielding is given by Eq. (5) as

$$\Delta K = -0.22E f \varepsilon_{ii}^T \sqrt{h}\, /(1-\nu) \qquad (13)$$

The supercritical plane strain toughness can thus be expressed in the following forms:

$$\Delta K_c = 0.22E f \varepsilon_{ii}^T \sqrt{h}\, /(1-\nu)$$

$$\Delta K_c / K_c = (\sqrt{3}/12\pi)(1+\nu) E f \varepsilon_{ii}^T / \bar{\sigma}^c (1-\nu) \qquad (14)$$

$$K_c / K_0 = [1 - (\sqrt{3}/12\pi)(1+\nu) \times E f \varepsilon_{ii}^T / \bar{\sigma}^c (1-\nu)]^{-1} \qquad (15)$$

If the transformation is not activated by the hydrostatic crack-tip field, but instead occurs in shear bands inclined at $\approx\pi/3$ to the crack plane ($\Omega \gg \tau$ in Eq. (6)), all of the deleterious transformations in front of the crack are excluded. Then, if the transformation strain is still hydrostatic, the supercritical ΔK_c increases to

$$\Delta K_c = 0.38E f \varepsilon_{ii}^T \sqrt{h}\, /(1-\nu) \qquad (16)$$

Zone profile considerations are thus of prime importance in determining the magnitude of the transformation toughening. It is also noted that, for conditions of plane stress, the zone width is predicted to be smaller, causing the toughness to diminish. When the transformation zone is large, the zone width may be affected by the previously transformed material and Eq. (12) does not apply. In this case a numerical solution has revealed the trend in the toughening ratio K_c/K_0 with $E f \varepsilon_{ii}^T / \bar{\sigma}^c$ depicted in Fig. 13. In particular, it is noted that "lock-up" occurs when $E f \varepsilon_{ii}^T / \bar{\sigma}^c = 30$. This phenomenon, first recognized by Rose,[24] has been elaborated by Amazigo and Budiansky.[15] Specifically, at lock-up, K at the crack tip tends to zero and the crack cannot propagate. In practice, under such conditions, an existing crack would arrest and new cracks would form and grow, leading to a damage mode of failure.

¶An extensively twinned particle with uniform twins and, thereby, no long-range shear strain.

Few toughened materials exhibit *supercritical* transformation. Generally, there is a gradient in the fraction of transformed material with the transformation zone, with the largest fraction present near the crack plane. Such conditions are referred to as *subcritical*. For this case, the toughness can be obtained by integrating the measured transformed fraction over the width of the zone.[9,10] Also, in some materials, the transformation is reversible. Such transformations can produce toughening, provided that hysteresis is involved.[8]

The equivalent approach for cracking toughness, based on *conservation integrals*, dictates that, for the frontal zone, the volume elements within the zone do not experience unloading. Consequently, the path-independent J integral applies and the relation

$$J = (1-\nu^2)K^2/E \qquad (17)$$

pertains for all line contours around the crack tip. Furthermore, because the elastic properties of the transformed and untransformed materials are essentially the same, contours around the tip (giving K_{tip}) and remote from the tip (giving K_∞) yield identical values of K: whereupon $K_{tip} = K_\infty$ and $\Delta K = 0$, as before. Conversely, when a fully developed zone exists (Fig. 10), the material within the zone, behind the crack tip, has experienced unloading, and a path-independent J does not apply. In this case, the appropriate conservation integral, I, has the same form as J at the tip

$$I = (1-\nu^2)K_{tip}^2/E \qquad (18)$$

but remote from the tip

$$I = [(1-\nu^2)\, K_\infty^2/E] - 2\int_0^h U(y)\, dy \qquad (19)$$

where $U(y)$ is the residual energy density in the wake. Equating the magnitude of the conservation integral for the near-tip and remote paths gives

$$K_\infty^2 = K_{tip}^2 + [2E/(1-\nu^2)] \int_0^h U(y)\, dy \qquad (20)$$

or

$$\Delta \mathcal{G}_c = 2\int_0^h U(y)\, dy \qquad (21)$$

The integral in $U(y)$ can be simply related to the elemental stress–strain curve (Fig. 9). Specifically, material in the process zone undergoes a complete loading and unloading cycle as the element translates from the front to the rear of the crack tip during crack advance. Hence, each element in the wake is subject to the residual stress work contained by the hysteresis loop (Fig. 9). Consequently, by appreciating that the wake is subject to a residual compression, the residual energy density can be readily evaluated as[10]

Notation

α	Linear thermal expansion coefficient
β	Transition parameter
Γ_i	Fracture energy of interface
Γ_m	Fracture energy of matrix
Γ_f	Fracture energy of fiber
ε_{ij}	Strain-tensor
ε_{ij}^T	Stress-free strain
δ_{ij}	Kronecker delta
η	Microcrack density parameter
σ_{ij}	Stress tensor
σ_{ij}^*	Critical stress for transformation
σ_0	Steady-state matrix cracking stress in composite
σ_e	Equivalent stress
σ_u	Ultimate strength of composite
σ	Applied stress
$\bar{\sigma}$	Mean stress
τ	Shear resistance of interface *after debonding*
θ_T	Misfit strain for microcracking
χ	Ductile reinforcement toughening parameter
μ	Friction coefficient
ν	Poisson's ratio
$\bar{\nu}$	Poisson's ratio for microcracked body
A_0	Reference area (1 m²)
B	Bulk modulus
$\bar{B}$	Bulk modulus of microcracked body
c	Microcrack dimension
d	Debond length
E	Young's modulus of composite
E_m	Young's modulus of matrix
E_f	Young's modulus of fiber
F	Nondimensional crack closure force
f	Volume fraction
G	Shear modulus
$\bar{G}$	Shear modulus of microcracked body
$\mathcal{G}$	Strain energy release rate
$\mathcal{G}_c$	Critical strain energy release rate for the composite
$\Delta\mathcal{G}_c$	Increase in toughness of composite above matrix toughness
h	Process-zone width
h_p	Fiber pullout length
I	I integral

J	J integral
K	Stress intensity factor
K_{tip}	Crack-tip stress intensity factor
K_∞	Stress intensity factor associated with applied loads
K_c	Critical stress intensity factor for composite
K_0	Critical stress intensity factor for crack-tip extension
ΔK	Crack shielding stress intensity factor
ΔK_c	Increase in critical stress intensity factor above matrix value
l	Slip length
L	Bridging-zone length
L_g	Gauge length
m	Shape parameter for fiber strength distribution
n	Work hardening rate
p	Axial residual axial stress in the *matrix* in aligned fiber composite
q	Residual stress normal to interface in fiber composite
R	Reinforcement radius
s	Saturation matrix crack spacing
s_{ij}	Deviatoric stress
S	Fiber strength
S_0	Scale parameter for fiber strength distribution
t	Stress acting on reinforcement between crack surfaces
U	Residual stress work
u	Crack opening displacement
u_c	Crack opening upon reinforcement rupture
Y	Uniaxial yield strength

$$U(y) = \bar{\sigma}^c \varepsilon_{ii}^T f + \frac{B^*(\varepsilon_{ii}^T f)^2}{2(1 - B^*/B)} + \frac{E(\varepsilon_{ii}^T f)^2}{9(1-\nu)} \quad (22)$$

where B^* is the slope of the stress–strain curve of the transforming material. The three terms in Eq. (22) derive from the areas I, II, and III under the stress–strain curve depicted in Fig. 9. The latter two terms cancel when

$$B^* = -2E/3(1+\nu)$$

$$\equiv -4G/3 \quad (23)$$

and Eq. (21) for the toughening is then identical to Eq. (4). This condition for B^* applies when the transformation is *supercritical*.[10]

The preceding discussion has referred exclusively to *supercritical* transformations, wherein all particles within the zone transform. Subcritical transformations are characterized by a transformation slope $B^* > -4G/3$. Some typical results determined numerically for the dilatational transformation are plotted in Fig. 14.[10]

Resistance-curve behavior is inevitable in transformation-toughened materials, because initial crack growth is largely unaffected by transformations produced by the stationary crack. The slope of the resistance curve (the tearing modulus) is governed by the current geometry of the zone, which depends on zone evolution.[12,15] Consequently, toughening curves can only be calculated by applying incremental crack-growth methods. Such analysis reveals that the zone initially widens as the crack extends and eventually reaches a steady-state crack width (Fig. 15). The actual zone morphology and, thus, the shape of the resistance curve, depend on the transformation criterion and on the flow rule. Calculations based on a dilatational law indicate a large tearing modulus and a peak prior to steady state (Fig. 16).[12] The peak is most pronounced for the supercritical condition when the zone height is large. The existence of the peak is not physically obvious but may be rationalized by appreciating that the rising resistance curve and the steady-state resistance have a separate dependence on the frontal-zone shape evolution and are thus not uniquely connected. The occurrence of a peak fracture resistance coincides with a peak in zone height. Such zone height peaks have been observed by experiment.[22]

The resistance curves are also dependent on the length of the crack, resulting in *short crack effects* which influence trends in strength.[12] For crack lengths in the range $a \lesssim 5h$, interaction between the zones at the opposite crack tips reduces the zone shielding. Consequently, the optima in strength and toughness are not usually coincident. Property optimization thus involves consideration of crack-length effects, as well as resistance-curve considerations.[26]

(B) Microcrack Toughening

(i) Basic Features

The phenomenon of microcrack toughening was postulated more than a decade ago,[27-30] and, indeed, a range of materials exhibit trends in toughness with particle size, temperature, etc., qualitatively consistent with this mechanism. However, the mechanism has only been rigorously identified and validated for various two-phase ceramics, including Al_2O_3 toughened with monoclinic (m) ZrO_2[31] and SiC toughened with TiB_2.[32] The fundamental premise concerning the mechanism is depicted in Fig. 17. Microcracks occur *within regions of local residual tension*, caused by thermal expansion mismatch and/or by transformation.[33,34] The microcracks also occur along the lowest fracture energy paths and locally relieve the residual tension. Consequently, a dilatation occurs governed by the volume displaced by the microcrack. Furthermore, the microcracks reduce the elastic modulus within the microcrack process zone. The elemental stress–strain curve for a microcracking solid thus has the form depicted in Fig. 17. The hysteresis dictated by this curve, when the microcracks are activated by the passage of a macrocrack, constitutes the change in toughness, as elaborated below. However, this contribution is partially counteracted by a degradation of the material ahead of the microcrack. The full extent of the degradation is presently unknown.

The basic material quantities that allow microcracking (residual stress and low fracture energy interfaces) also lead to grain bridging, as described in Section II (3). Often, therefore, both microcracking and bridging operate simultaneously to a relative extent that depends on features of the microstructure. An important measurement that distinguishes the mechanism is the size of the microcrack process zone. The techniques that have the best capability for characterizing this zone are the scanning acoustic microscope (SAM), which allows measurement of the elastic modulus with high spatial resolution,[35] and transmission electron microscopy (TEM). For example, the SAM technique has recorded a small process zone in a polycrystalline Al_2O_3, but a substantial zone in a glass-ceramic material, whereas TEM has identified microcrack process zones in Al_2O_3/m-ZrO_2 and in SiC/TiB_2.

The crack shielding caused by microcracks can be conveniently separated into dilatational and modulus contributions. The former depends on the process-zone size and shape, whereas the latter depends only on the zone shape. The *dilatational contribution* to K_{tip} from the residual field has precisely the same form as that associated with transformations, but with $f\varepsilon_{ii}^T$ replaced by θ_T. This contribution thus depends on zone size and shape, as in the case of transformation toughening. For example, when the

microcrack nucleation condition involves a critical *normal* stress, the steady-state toughening is[34]

$$\Delta K_c = 0.40 E\theta_T \sqrt{h} \tag{24}$$

whereas, for a critical *mean* stress

$$\Delta K_c = 0.32 E\theta_T \sqrt{h} \tag{25}$$

where θ_T is now the misfit strain caused by microcracks (analogous to $f\varepsilon_{ij}^T$). By contrast, the toughening imparted by the modulus reduction *depends on zone shape, but not on zone size*. Following Hutchinson,[34] the asymptotic *modulus* contribution is[34]

$$(1-\nu)\Delta K_c/K_c = (k_1 - \tfrac{5}{8})(G/\bar{G} - 1) + (k_2 + \tfrac{3}{4})(\bar{\nu}G/\bar{G} - \nu) \tag{26}$$

where k_1 and k_2 depend on the microcracking criterion. Values of $\Delta K_c/K_c$ can be obtained by simply inserting $G/\bar{G}$ and $\bar{\nu}$ into Eq. (26). Typical results for the steady-state toughening are, for a critical normal stress and penny-shaped microcracks

$$\Delta K_c/K_c = 1.42\eta \tag{27}$$

with η being a measure of the microcrack density, defined following Eq. (30). In general, the ΔK_c due to dilatation and modulus effects are not additive: interaction terms are involved.

(ii) Constitutive Law

The reduction in elastic moduli caused by microcracks, as well as the permanent strain governed by release of the residual stress, depend upon microstructure. Characteristic constitutive laws are illustrated for two important cases consisting of spherical particles subject to either residual tension or residual compression. For the former case, the microcracks occur either within the particle or at the interface, whereas for the latter, the matrix develops microcracks. Results for these cases have been derived for materials having homogeneous elastic properties prior to microcracking. For *particles subject to residual tension*, in which penny-shaped microcracks form (Fig. 17), the volume of each opened microcrack is[34]

$$\Delta V = (16R^3/3)(1-\nu^2)\sigma_{ii}^P/E \tag{28}$$

where

$$\sigma_{ii}^P = 2E\varepsilon_{ii}^T/9(1-\nu) \tag{29}$$

R is the particle radius and ε_{ii}^T the misfit strain between particle and matrix. This volume increase dictates the permanent strain, such that the *microcrack misfit strain* becomes

$$\theta_T = (16/3)(1-\nu^2)\eta\sigma_{ii}^P/E \tag{30}$$

where $\eta = N\langle R^3\rangle$ is the number density of microcracked particles, with N being the number of microcracked particles per unit volume. Solutions for the elastic moduli of microcracked bodies establish the modulus effect[34] as

$$G/\bar{G} = 1 + (32/45)(1-\nu)(5-\nu)\eta/(1-\nu)$$

$$B/\bar{B} = 1 + (16/9)(1-\nu^2)\,\eta/(1-2\nu) \tag{31}$$

where the bar refers to microcracked material.

For particles in residual compression, the corresponding constitutive law depends sensitively on the response of the interface to the microcrack. For the one material studied thus far (Al_2O_3/ZrO_2), some debonding occurs at the interface and the basic parameters derived for the microcracks are (Fig. 18)

$$\theta_T = 3.6(u_R/R)\eta/\zeta^2 \tag{32}$$

where u_R is the residual microcrack opening of the interface, as affected by the debond length, d, and

$$\zeta = c/R$$

where c is the microcrack length. The above results may be used in conjunction with Eqs. (25) and (26) to predict toughening.

(iii) Toughness Correlation

Microcracking in various zirconia-toughened alumina (ZTA) materials and in SiC/TiB_2 has been systematically studied by preparing thin foils at various distances, y, from a macrocrack.[31,32] For the former, radial matrix microcracks were observed. All such radial microcracks occurred along grain boundaries in the Al_2O_3. Usually, the interface between the Al_2O_3 and ZrO_2 was debonded at the ori-

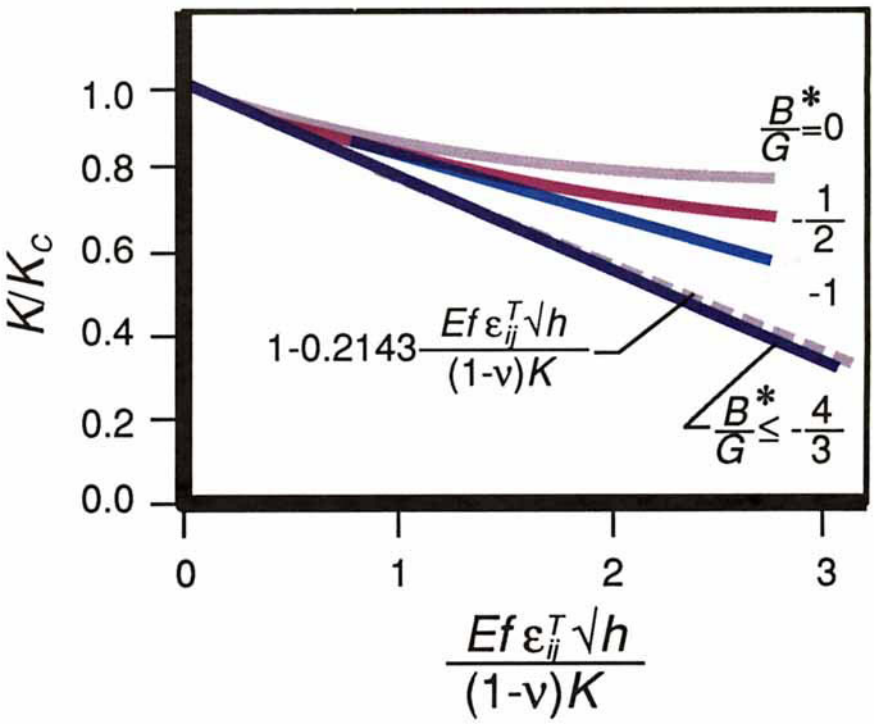

Fig. 14. Ratio of near-tip to remote stress intensity factors. The dashed line is the asymptotic result for small ε_{ij}^T.

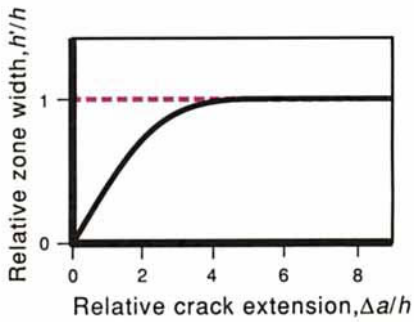

Fig. 15. Dependence of relative zone width on relative crack extension.

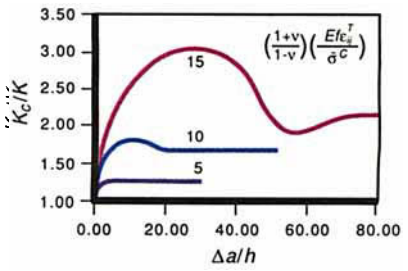

Fig. 16. Theoretically predicted ratio of (relative) toughness to crack extension.

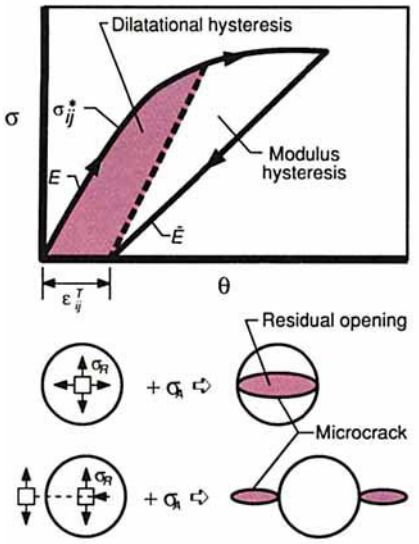

Fig. 17. Basic concepts of microcrack toughening.

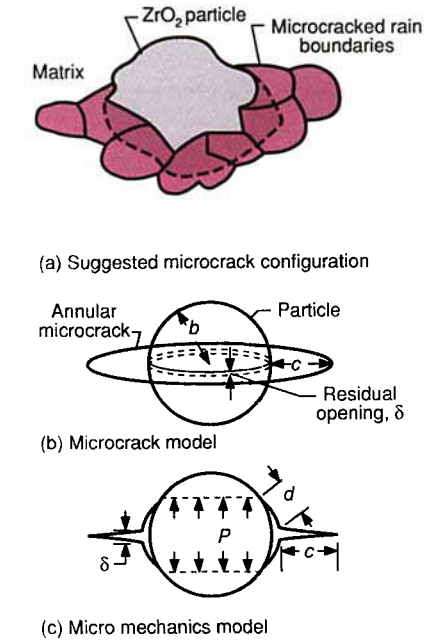

Fig. 18. Microcrack model used to measure crack densities and to analyze the changes in crack volume and elastic modulus: (A) schematic drawing of a typical configuration, (B) microcrack model used for analysis, and (C) mechanics model.

gin of the microcrack. The detectibility of radial microcracks depended on their inclination with respect to the incoming electron beam. Trends in the visibility of microcracks upon tilting around one axis indicated that tilting in all directions would be needed to detect each microcrack present in the foil. However, tilting in the TEM is limited to $\pm 45°$ in all directions, so that only 0.3 of the solid angle is covered. Therefore, the fraction of detectable microcracks is limited to ≈ 0.3.

Subject to this detectability limitation, large regions of TEM foils of known thickness have been investigated. One example is shown in Fig. 19, wherein all microcracks observable under different tilting conditions are marked. It is noted, on the average, that at least two microcracks emanate from each *m*-ZrO_2 particle. In most cases, the microcracks terminate at the Al_2O_3 grain triple junctions. The associated projected length, l, of each microcrack has been measured and related to the radius, b, of the originating *m*-ZrO_2 particle.

The utility of microcrack length measurements is facilitated by defining a representative geometry and determining the related microcrack density parameter, η, introduced by Budiansky and O'Connell.[36] Evaluation of the microcrack profiles observed by tilting suggests that each ZrO_2 particle is circumvented by a radial microcrack, consistent with the symmetry of the residual strain field around each particle. The model depicted in Fig. 18 has thus been used for further analysis.

The microcrack density determined from the frequency distribution of projected microcrack lengths (Fig. 20) diminishes with distance from the crack plane. A maximum density, η_s, adjacent to the crack surface suggests a *saturation value*, governed by the total ZrO_2 particle content, as needed to use the shielding formulation. The decrease with distance y is approximately linear, such that

$$\eta \approx \eta_s(1 - y/h) \tag{33}$$

where h is the process-zone width. A similar trend was found for SiC/TiB_2.[32] Based on the above results, the residual strain contribution to the shielding has been determined as $\Delta K_d = -2.5 \pm 1$ MPa·m$^{1/2}$. The modulus-reduced shielding is obtained as $\Delta K_m = -5 \pm 2$ MPa·m$^{1/2}$. Simple addition of the dilatational and modulus contributions would indicate toughening, ΔK_c, of ≈ 7.5 MPa·m$^{1/2}$, sufficient to account fully for the measured toughness, ΔK_c, of ≈ 6 MPa·m$^{1/2}$. It should be appreciated, however, that the individual contributions to the shielding are relatively large and additivity is not strictly valid. Interaction effects should be taken into account before more rigorous comparisons between theory and experiment are attempted. It is of interest to note that the modulus reduction and dilatational contributions to the shielding are similar in magnitude. This is important because, although the former contribution cannot be readily changed (being governed almost entirely by the saturation microcrack density, η_s), the dilatational contribution may be enhanced by increasing both the process-zone size and the microcrack density within the zone. This may be achieved by control of the *m*-ZrO_2 particle-size distribution, through its influence on the nucleation of the microcracks.

Although progress has been appreciable, a number of substantive problems exist in the analysis of microcrack toughening, both experimental and theoretical. Among the problems are a poor fundamental understanding of the degradation caused by the microcracks directly ahead of the crack front and limited knowledge of the interactions between modulus and dilatational contributions to crack shielding, as well as experimental microcrack detectability limitations. These topics require further study before authoritative conclusions can be reached regarding toughening and before predictions of toughening trends can be rigorously contemplated.

(3) Bridging Mechanisms

Contributions to the toughness caused by reinforcing elements that bridge between the crack surfaces are conveniently separated into two types: ductile and brittle. The former refers to metal-toughened ceramics (cermets) and relies on high toughness and ductility to permit metal ligaments to exist and to contribute to toughness through plastic dissipation. However, when the bridging material is brittle, such that the toughness of the bridge is similar to that of the nonbridging (matrix) material, the occurrence of bridging is more subtle and requires either microstructural residual stress or weak interfaces or both. The former may be appreciated by noting that large local residual stresses caused by thermal expansion mismatch/anisotropy are capable of suppressing local crack propagation (Fig. 21) and, thereby, may allow intact ligaments to exist behind the crack front.[37] When these ligaments eventually fail in the crack wake, energy is dissipated as acoustic waves and causes toughening (Fig. 22). The latter may be understood by recognizing that low fracture energy interfaces (and/or grain boundaries) can cause the crack to deflect along those interfaces, again permitting intact ligaments. As the crack extends, further debonding can occur. Eventually, the bridging material fails, either by debonding around the end or by fracture. Following failure, frictional sliding may occur along the debonded surface. The energy dissipation upon crack propagation thus includes terms from the energy of the debonded interfaces, the acoustic energy dissipated upon reinforcement failure, and frictional dissipation during pullout (Fig. 22). These contributions

lead to a unified model of the fracture resistance of materials that exhibit bridging by brittle ligaments.

(A) Ductile Reinforcement Toughening

(i) Basic Features

Ductile reinforcements may profoundly increase the toughness. One contribution to the toughness derives from crack trapping,[38] another involves crack bridging,[13,39-41] and yet another involves crack shielding and plastic dissipation associated within a plastic zone.[42] The material systems that exhibit plasticity-induced toughening have three distinct microstructures: *isolated ductile reinforcements*, *interpenetrating networks*, and a *continuous ductile phase*. Isolated ductile reinforcement is exemplified by ductile fibers,[43-45] by Nb-alloy plates in TiAl,[46,50] and, probably, by ferrite in the quasi-cleavage of steels.[48] An example of an interpenetrating network is Al-alloy-reinforced Al_2O_3 produced by the Lanxide method.[49,50] The continuous ductile network case includes most metal-matrix composites and, probably, cemented carbides.[51] An important difference between the first two microstructures and the third concerns the potential for plastic strain in the composite outside the bridging ligaments. Plastic strain in the first two is limited by elastic strains in the elastic network. Consequently, experience and analysis confirm that crack bridging is usually the most potent mechanism when the ceramic phase is *continuous*, because the only ductile regions which experience extensive plastic strain are those segments that stretch between the crack surfaces in the bridging zone. The plastic dissipation in this bridging zone can be large and can provide a major increase in toughness. Conversely, a composite with a continuous metal network is subject to nonlinear power law deformation and can experience substantial plastic strain within a plastic zone. Consequently, the potential for appreciable plastic dissipation within a plastic process zone is much greater for this class of microstructure.

Understanding of the toughness generated by ductile ligaments is contingent upon the law that characterizes the stress/stretch relation, $t(u)$. Insights regarding the parameters that affect this relation can be gained from simplified analytical models. Complementary numerical solutions then allow determination of specific trends. Budiansky and co-workers[13,52] and Rose[53] analyzed *small-scale bridging*, in which bridge length is small in relation to crack length, specimen dimensions, and distances from the crack to the specimen boundaries. The stress/stretch relation depends strongly on the mode of failure of the ductile ligaments. A *small-scale* yielding analysis indicates that t should increase rapidly with *initial* crack opening. A large-strain necking analysis then reveals that, without debonding, the stress attains high initial levels because of the elastic constraint of the matrix, but should decrease as the crack opens and, furthermore, should depend sensitively on the work hardening rate. These simple results already provide the important insight that a *peak stress* exists at *small* crack openings, such that the plastic dissipation is dominated by the large strain (necking) regime (Fig. 23). The importance of interface *debonding* thereby becomes apparent, because debonds reduce the constraint, but increase the plastic stretch prior to failure. Numerical solutions obtained with prescribed initial debonds establish the salient trends (Fig. 23). Notably, the plastic dissipation increases systematically as d/R increases. Furthermore, if the debond *evolves* during crack opening, the dissipation is further enhanced. The above predictions are generally similar to experimental measurements, which confirm large stresses at small u and increased dissipation when debonding occurs.

The toughness attributed to bridging, based on Eq. (3), can be reexpressed in nondimensional form by noting that the flow stress scales with the uniaxial yield strength, Y, and that the plastic stretch is proportional to the radius of the cross section of the reinforcing ligaments, R; consequently, the asymptotic toughness is[40,41]

$$\Delta\mathcal{G}_c / fYR = \chi \qquad (34)$$

where χ is a "work-of-rupture" parameter that depends on the critical plastic stretch, u_c (or ductility), of the reinforcement and on the extent of the interface debonding, d. Values of χ have been obtained both by calculation and by experiment,[40] based on determinations of the area under the stress/stretch curve for the reinforcing ligaments. For a *well-bonded interface* ($d \approx 0$) and for ductile ligaments that fail by necking to a point, the resultant trend in χ with

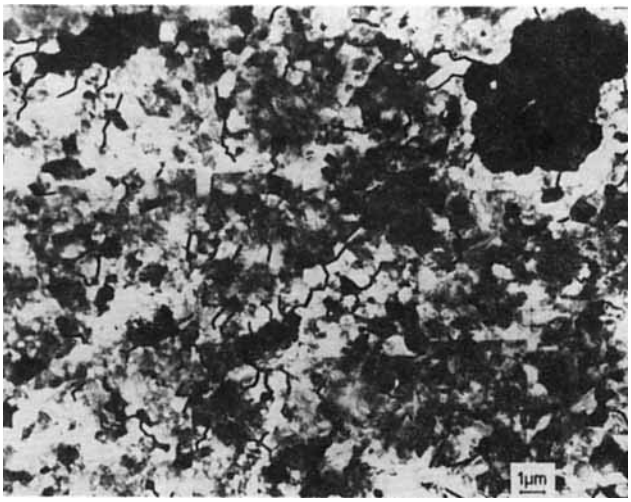

Fig. 19. TEM photograph with all observable microcracks marked.

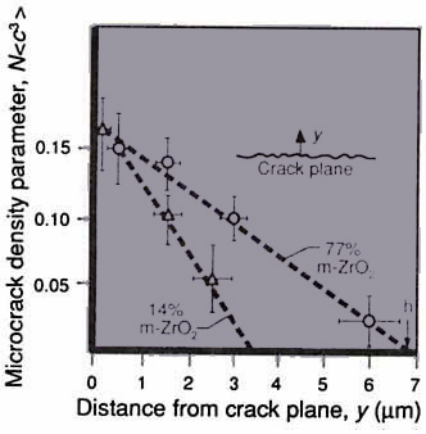

Fig. 20. Trends in the microcrack density parameter, $\eta = N\langle c^3 \rangle$, with distance y from the crack surface.

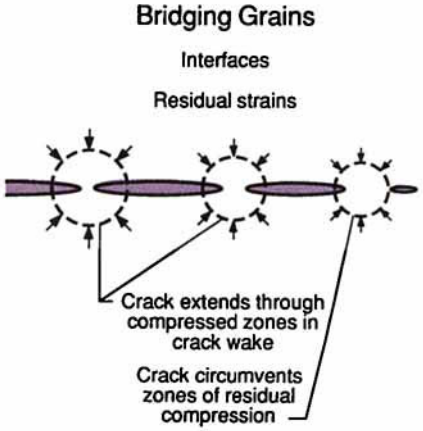

Fig. 21. Ligament formation allowed by residual stress.

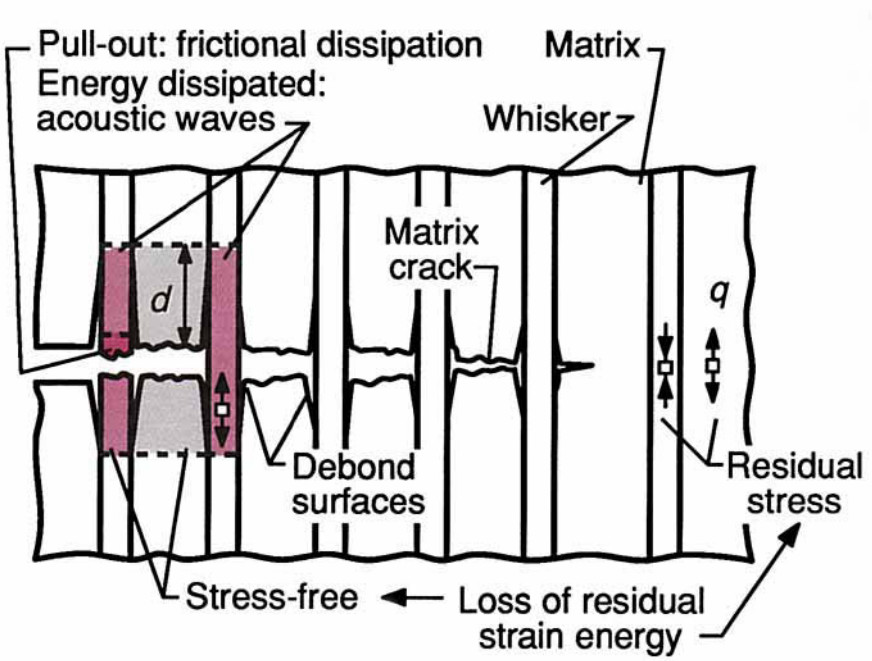

Fig. 22. Schematic indicating the various contributions to the steady-state toughness.

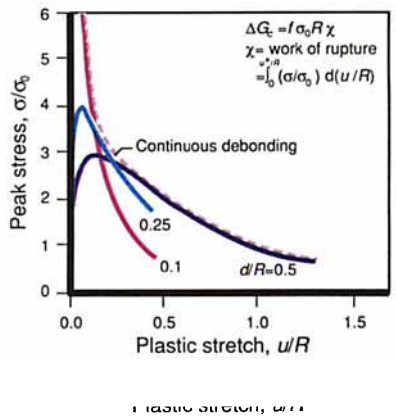

Fig. 23. Nondimensional stress versus stretch behavior and associated "work-of-rupture" χ for various debond lengths.

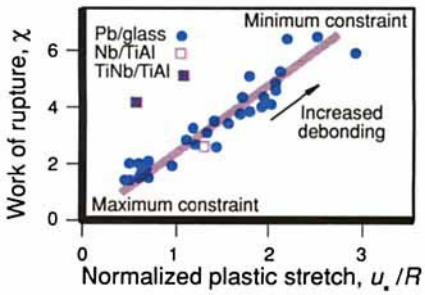

Fig. 24. Work of rupture as a function of plastic stretch measured for various ductile reinforcements.

work-hardening rate n indicates that χ is in the range 0.3 to 1. Less-ductile ligaments that rupture prematurely by profuse hole nucleation have correspondingly smaller values of χ. Systems subject to *debonding* exhibit larger χ and approach 8 for large d/R. Experimental results have indicated that trends in χ and d are reflected in a plot of χ with relative plastic stretch u_c/R (Fig. 24).

(ii) Toughness Correlations

The basic nondimensional solution (Eq. 34) can be used both to rationalize toughness measurements and to develop a predictive capability. For purposes of the former, Y and n can be inferred either from a TEM characterization of the microstructure[50] or from microhardness measurements (Elliott *et al.*[48]), while f, R, u_c, and d can be determined by quantitative SEM of the fracture surface.[50] Comparison between theory and experiment is most readily achieved by reexpressing Eq. (34) in the form

$$\Delta\mathcal{G}_c = f\,YR\chi\,\overline{(u_c/R)} \qquad (35)$$

To use this result, Y is first obtained, followed by evaluation of χ, using $\overline{u_c/R}$. Thereafter, $\Delta\mathcal{G}_c$ is examined for consistency by comparison with the experimentally determined value. For Lanxide composites of Al_2O_3 reinforced with Al, the experimental information is as follows: The yield strength has been evaluated by noting that the alloy contains Al-Cu precipitates which behave as impenetrable obstacles (Fig. 25). Consequently, their influence on yielding should be represented by Orowan hardening, wherein the precipitates locally block the passage of dislocation, causing the flow strength to be inversely proportional to the precipitate spacing. Inserting the measured precipitate spacing ($\lambda \approx 100$ nm), the yield strength is $Y \approx 220$ MPa. This value is comparable to typical values quoted for Al alloys precipitation hardened with Cu. Stereo measurements have been used to evaluate the plastic stretch to failure, u_c. The normalized *plastic stretch*, u_c/R, varied appreciably between ligaments. However, there was no systematic dependence on either the ligament dimension, R, or the aspect ratio: the mean stretch was $\overline{u_c/R} = 1.6$. The plastic stretch to failure indicates that χ is in the range 2 to 3.5. Substituting the above values of Y and χ into Eq. (35) and noting that $f = 0.2$ and $R = 2.0$ μm, $\Delta\mathcal{G}_c$ is calculated as 170 to 300 J·m^{-2}. Consequently, there is acceptable agreement with the measured value of 150 to 200 J·m^{-2}. Such behavior is consistent with the interpenetrating network microstructure.

For cemented carbide materials, the contribution from bridging deduced from the measured zone sizes is found to be relatively small[54,55] ($\Delta\mathcal{G}_c \approx 40$ J·m^{-2}) for reasonable choices of the flow stress of the Co alloy, whereas the overall measured toughness is $\mathcal{G}_c \approx 400$ J·m^{-2}. Consistent with this interpretation, measurements of plastic zones indicate zone sizes in the range $h \approx 40$ μm.[42] It is supposed that dissipation is appreciable in this zone and that this may be the predominant contribution to the toughness of these materials.

(B) Fiber/Whisker Reinforcement

(i) Basic Features

Practical ceramic-matrix composites reinforced with *continuous fibers* exhibit the failure/damage behaviors sketched in Fig. 26. The composite properties are known to be dominated by the interface, and bounds must be placed on the interface debonding and sliding resistance to have a composite with attractive mechanical properties. The strong dependence of ceramic-matrix composite properties on the mechanical properties of the interface generally demands consideration of fiber coatings and/or reaction product layers. Residual stresses caused by thermal expansion differences are also very important.

The specific microstructural parameters that govern Mode I failure are the relative fiber/matrix interface debond toughness, Γ_i/Γ_f, the misfit (thermal expansion) strain between fiber and matrix, ε_{ii}^T, the friction coefficient at the debonded interface, μ, the statistical parameters that characterize the fiber strength, S_0 and m, the matrix toughness, Γ_m, and the fiber volume fraction, f. The prerequisite for toughness is that $\Gamma_i/\Gamma_f \lesssim 1/4$ to allow crack-front debonding (Fig. 27). Subject to this requirement, the misfit strain must be small ($\varepsilon_{ii}^T \lesssim 3 \times 10^{-3}$) and preferably negative,

such that the interface is in tension. Furthermore, for a continuous fiber, the friction coefficient along the debonded interface should be small. The ideal fiber properties include a high median strength (large S_0) and large variability (small m), as needed to encourage large pullout lengths. When Γ_i/Γ_f and μ are both small, experience has indicated that the tensile stress–strain behavior illustrated in Fig. 26(A) is obtained. Three features of this curve are important: matrix cracking at a stress σ_0, fiber-bundle failure at σ_u, and pullout. Conversely, larger Γ_i/Γ_f and μ cause the stress–strain curve to become linear (Fig. 26(B)). The ultimate strength then coincides with the propagation of a single dominant crack.

Present understanding of debonding is consistent with the following sequence of events during matrix crack propagation. Initial debonding along the interface at the crack front requires that Γ_i/Γ_f be small enough to lie within the debond zone depicted in Fig. 27.[56] Furthermore, the extent of debonding is typically small when residual compression exists at the interface, but can be extensive when the interface is in residual tension and the fibers are smooth. Further debonding is usually induced in the crack wake[57] (Fig. 28). The extent of this debonding is governed largely by the residual field. Residual radial tension results in unstable conditions and encourages the extensive debonding of smooth fibers. Residual compression and/or an irregular fiber morphology cause stable debonding,[58] with the extent determined by the friction coefficient and the roughness of the debonded interface. Subsequent fiber fracture involves the statistics of fiber failure,[59] subject to an axial stress governed by the sliding resistance of the debonded interface. The above sequence suggests that, although debonding is a prerequisite for high toughness, the properties of the composite are dominated by the sliding resistance of the debonded interface, which dictates the major contribution to toughness caused by pullout. The locations of fiber failure that govern the pullout distributions can be determined from the stresses on the fibers, using concepts of weakest-link statistics. Analysis of this phenomenon has been performed for composites having debonded interfaces subject to a constant sliding stress, τ.[59] The magnitude of τ governs the load transfer from the fiber to the matrix. Large values of τ cause the fiber stress to vary rapidly with the distance from the matrix crack and induce fiber failure close to the crack, leading to small pullout lengths, h_p. Conversely, small τ results in large h_p.

Various observations of crack interactions with fibers are supportive of the above rules. In particular, experiments on glass and glass-ceramic-matrix composites reinforced with SiC fibers reveal that materials with a C interlayer satisfy debonding requirements (Fig. 29) and also have small τ and thus demonstrate extensive pullout.[60-62] Conversely, composites having a continuous SiO_2 layer between the matrix and fiber exhibit matrix crack extension *through* the fiber without debonding[62,63] (Fig. 30). Experiments on these composites and on whisker-reinforced composites also confirm the strong influence of τ. Notably, systems which debond but do not slide readily (because of either a high friction coefficient or morphological irregularity) exhibit small pullout lengths and moderate toughness. Such behavior is exemplified by LAS††/SiC composites with oxide interphases and by various whisker-reinforced materials, respectively.

Tough composites can be obtained by creating the appropriate interphases between the fiber and matrix, either by coating or, in situ, by segregation/interdiffusion. The most common approach is the use of a dual coating: the inner coating satisfies the debonding and sliding requirements, while the outer coating provides protection against the matrix during processing. However, the principal challenge is to identify an inner coating that has the requisite mechanical properties while also being thermodynamically stable in air at elevated temperatures.

(ii) Constitutive Laws

The mechanical properties of uniaxially reinforced composites are largely governed by the relationships between the opening of a matrix crack, u, and the stresses, t, exerted on the crack by the intact bridging fibers and the failed fibers as they pull out. The traction $t(u)$ is well-known for composites in which debonding occurs easily (very small Γ_i/Γ_f) and which also slide easily along the debonded interface (small τ). For other cases, reliable $t(u)$ functions have yet to be elucidated. Easy debonding and sliding provide a crack-opening function that depends on the sign of the misfit strain, as well as the roughness of the debond interface, through their effect on the sliding resistance. For instance, sliding can be described by a Coulomb friction law

$$\tau = \mu q \tag{36}$$

where μ is the friction coefficient and q the nominal residual compression normal to the interface. At the simplest level, q is set by the residual misfit strain and the fiber/coating morphology, such that τ is essentially invariant. In this case, prior to the incidence of fiber failure, t and u are related by[17,18]

$$t = \frac{2fE}{E_m(1-f)}\left[\frac{\tau E_f}{R}\right]^{1/2} u^{1/2} \tag{37}$$

Equation (37) has been used to describe the mechanical behaviors that are obtained while the fibers are largely intact.

††Lithium aluminum silicate.

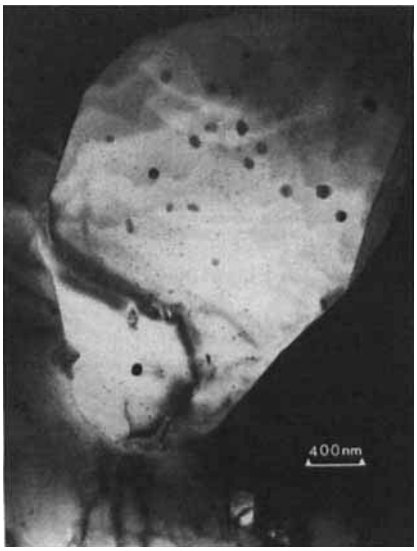

Fig. 25. Bright-field TEM view of the precipitates in the Al alloy that cause hardening.

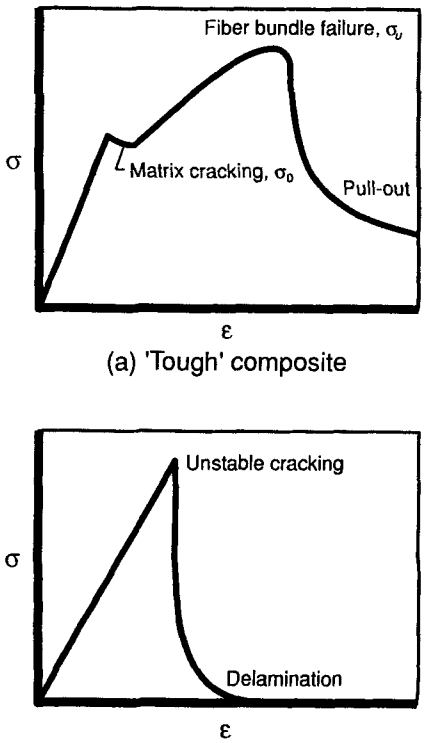

Fig. 26. Schematic illustrating the range of stress–strain characteristics exhibited by ceramic-matrix composites.

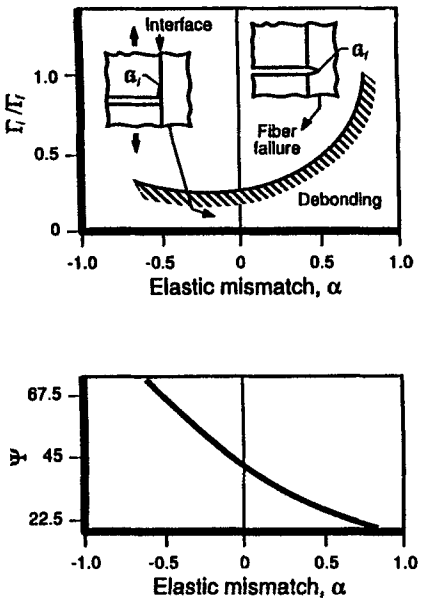

Fig. 27. Fracture energy requirements for crack-front debonding.

At another extreme, when all of the fibers have failed, the traction on any fiber is[59,63]

$$t_i = 2f\tau(h_i - u)/R \tag{38}$$

where h_i is the distance from the matrix crack plane at which that fiber failed.

More difficult problems to address concern the incidence and location of fiber failure. This has been regarded as a problem in weakest-link statistics,[64] whereupon the function $t(u)$ depends upon the statistical parameters S_0 and m in addition to the variables contained in Eq. (37). The expressions are unwieldy and are not reproduced here, but can be located in the article by Thouless and Evans.[59] Some trends, expressed in nondimensional form, are summarized in Fig. 31. The small displacement behavior is dominated by the intact bridging fibers, whereas the long tail is governed by the pullout of failed fibers.

Another level of complexity is involved when the interface stress q_N varies with the loads t on the fiber. A simplified result obtained using a modified shear lag approach suggests the following features[58] ($E_f = E_m = E$ and $\nu_f = \nu_m = \nu$):

$$u/R \approx (\varepsilon_{ii}^T/\mu)[F(1+F)/(1-\nu F)] \times (1-\nu+\nu f)/(1-f) \tag{39}$$

where

$$F = t/\varepsilon_{ii}^T E$$

with ε_{ii}^T being the misfit strain which causes the interface to be in residual compression. Equation (39), although approximate, has several salient features. In particular, as expected, crack opening is inhibited by large values of the friction coefficient. Furthermore, as $F \to 1/\nu$, the fiber and matrix surface separate, leading to unrestricted crack opening. Additional complexity is involved when debonding and sliding occur simultaneously. Some preliminary results for such behavior exist, but are not addressed here. It is simply noted that, in such cases, the fracture energy of the coating becomes another parameter of interest.

The location of fiber failure vis-a-vis the matrix crack plane is of critical importance because this location governs the pullout length h_p. Both theory[59] and experiment[65] suggest that, for aligned reinforcements, h_p is governed by weakest-link statistics. For the simplest case, wherein the sliding stress τ remains constant, an expression for the mean pullout length has been derived as[59]

$$(2h_p/R)^{m+1} = [1/2\pi(m+1)^m](A_0/R^2) \times (S_0/\tau)^m \Gamma[(m+2)/(m+1)] \tag{40}$$

where Γ in this expression is the gamma function and A_0 is a reference area for the fibers (usually set equal to 1 m²). Consequently, for aligned fibers, it is evident that h_p/R is essentially governed by S_0/τ: *high fiber "strength" and low sliding resistance encourage large pullout lengths.* Corresponding trends for inclined fibers are unknown.

(iii) Matrix Cracking Stress

The stress σ_0 at which *matrix cracking* occurs has been the most extensively studied behavior in ceramic-matrix composites. For composites in which the residual stress normal to the interface, q_N, is tensile and the interface properties can be effectively represented by a unique sliding stress, τ, Eq. (37) may be used to derive the lower-bound, steady-state matrix cracking stress.[17]

$$\frac{\sigma_0}{E} = \frac{\sigma^*}{E} - \frac{p}{E_m}$$

where

$$\frac{\sigma^*}{E} = \left[\frac{6f^2 E_f \tau \Gamma_m}{(1-f)EE_m^2 R}\right]^{1/3} \tag{41}$$

with p being the axial residual stress in the matrix. This result is *independent* of the matrix crack length because the crack is "fully" bridged by fibers and applies when the initial crack is larger than the fiber spacing.[18] Measurements performed on many different glass- and ceramic-matrix composites (Fig. 32) reinforced with Nicalon fibers have verified that Eq. (28), in fact, provides an adequate representation of matrix cracking provided that $\tau \lesssim 20$ MPa.[62] Values of τ in this range have been demonstrated for fibers coated with either C or BN, as elaborated below. For these systems, it is recognized that τ depends on the misfit strain, and, consequently, for the simple case wherein τ and q_N are related through a friction coefficient (Eq. (36)), the matrix cracking

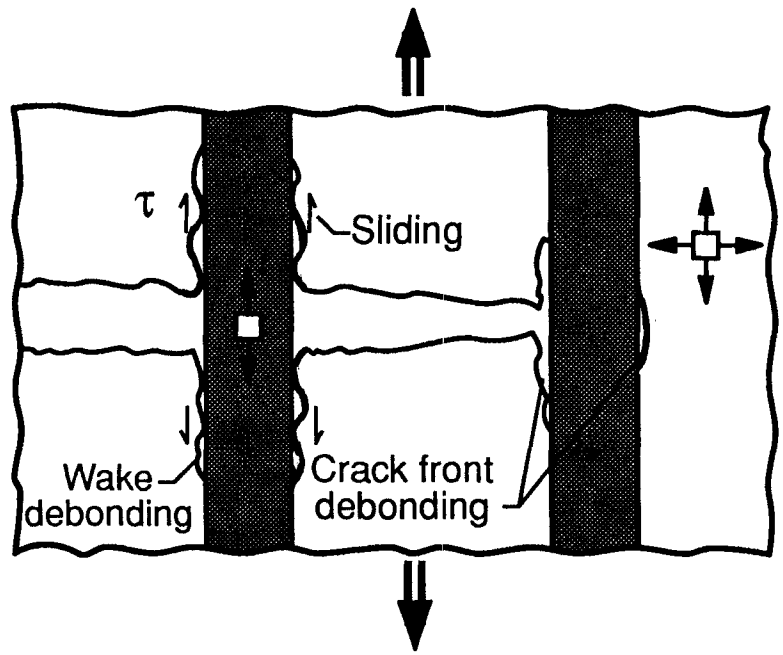

Fig. 28. Schematic illustrating the initial debonding of fibers at the crack front, as well as fiber debonding and sliding in the crack wake.

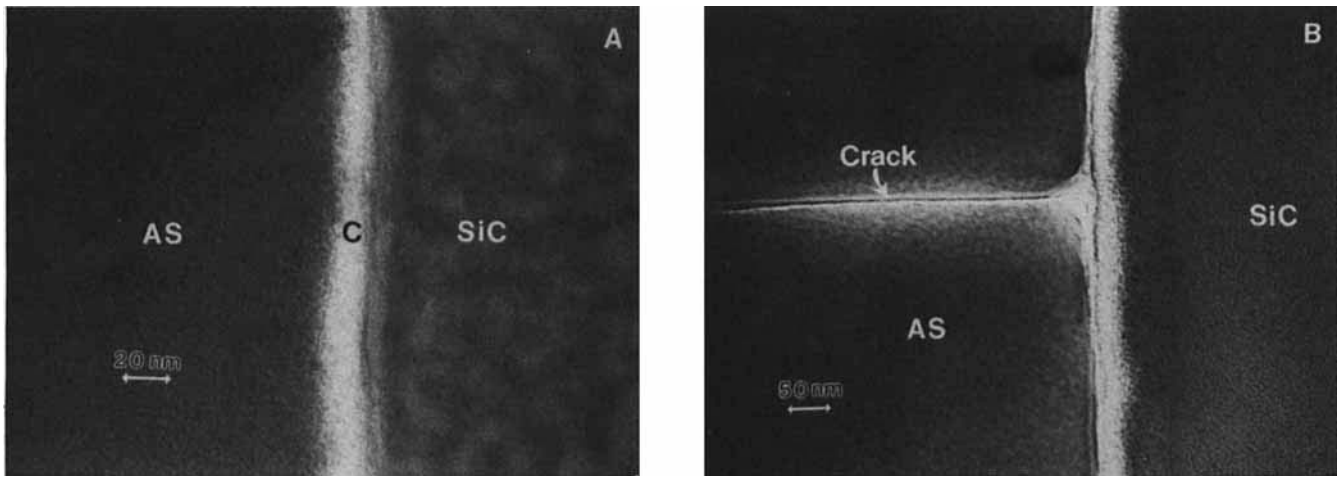

Fig. 29. Crack-front debonding in a Nicalon-fiber-reinforced aluminosilicate-glass-matrix composite.

stress exhibits a *maximum* $\hat{\sigma}_0$ given by[17]

$$\hat{\sigma}_0/E = (2/3)[2f\mu\Gamma_m/(1+E/E_f)E_mR]^{1/2} \quad (42)$$

This result has evident implications for material design.

More detailed diagnosis of matrix cracking confirms that Eq. (41) is a lower bound for the onset of cracking. Further cracking occurs as the stress is raised above σ_0, resulting in a periodic crack array (Fig. 33).[16] The crack spacing reaches a *saturation value, s,* when the stress everywhere in the "matrix blocks" between cracks becomes smaller than that applied stress. The magnitude of the saturation crack spacing is governed by the sliding stress, τ, such that τ and s are related by[62]

$$\tau = 1.34[(1-f)^2\Gamma_m E_f E_m R^2/fEs^3]^{1/2} \quad (43)$$

Consequently, the matrix cracking stresses can be expressed in terms of the crack spacing as

$$\sigma_0 = 2\left[f\frac{\Gamma_m E_f E}{E_m s}\right]^{1/2} - p\frac{E}{E_m} \quad (44)$$

The crack spacing clearly provides an approach for estimating τ and for establishing a self-consistent description of matrix cracking.

(iv) Toughness

In reinforced ceramics which fracture by the growth of a single dominant flaw in Mode I, there are four effects which influence toughness.[66] *Debonding* generates new surface and contributes positively to toughness. *Frictional dissipation* upon pullout results in local heating and again contributes positively. *Residual stresses* present in the material are partially relieved by matrix cracking and debonding and thus detract from the toughness. Finally, when the fibers fail, some of the *elastic energy* stored in the fiber is dissipated through acoustic waves and appears as a positive contribution to toughness. The above effects are indicative of *resistance-curve behavior*, because each contribution is only fully realized when the fibers fail and pull out. The full details of the increase in the fracture resistance can be calculated from the crack surface tractions $t(u)$ by applying Eq. (3). A useful simplification for further discussion is the peak (or asymptotic) toughness that is obtained when each mechanism exerts its maximal contribution. At the simplest, physically relevant level, this toughness is given by[66]

$$\Delta\mathcal{G}_c \approx fd[S^2/E - E(\varepsilon_{ii}^T)^2 + 4\Gamma_i/R(1-f)] + 2\tau f h_p^2/R \quad (45)$$

The first term is a bridging contribution that derives from the stored strain energy dissipated as acoustic waves, with S being the reinforcement "strength." The second term is the loss of residual strain energy caused by matrix crack extension and debonding. The third term reflects the new "surface area" caused by debonding, and the fourth term is the pullout contribution, dissipated by frictional sliding of the interfaces.

Experience indicates that the residual strain term is small in systems of practical utility and can often be neglected. The largest potential for toughness resides in the pullout term, *provided that* h_p/R *is large.* An extreme range of pullout behaviors is apparent among the available range of fiber- and whisker-reinforced ceramics, resulting in wide variations of toughness. Understanding pullout thus dominates our capability for producing ceramic composites having exceptional toughness. The dominance of toughness by pullout provides a focus for specifying those properties of the fibers and fiber coatings that optimize the frictional dissipation. For aligned reinforcements, wherein weakest-link statistics govern the pullout length, an explicit dependence of toughening on

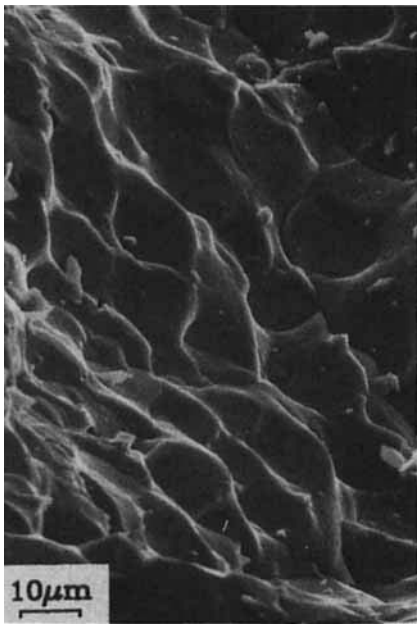

Fig. 30. Fracture surface indicating fracture through the fiber in a silica/SiC-fiber composite.

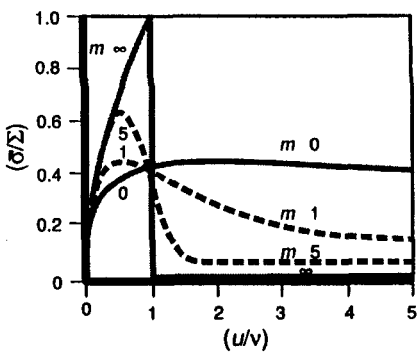

Fig. 31. Nondimensional crack closure stress as a function of crack opening.

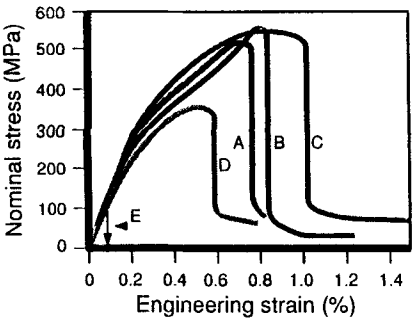

Fig. 32. Tensile stress–strain curves for a range of glass- and glass-ceramic-matrix composites reinforced with SiC (Nicalon) fibers.

fiber strength and sliding resistance is predicted.[59] Physically stated, *high fiber strength and low sliding resistance combine to maximize the frictional dissipation by inducing sliding over the largest possible fiber surface area.* The inverse dependence of pullout toughening on τ emphasizes the need to control and understand sliding. Some of the qualitative features are depicted in Fig. 34, illustrating the importance of the fiber morphology, the misfit strain, and the friction coefficient.

Nonaligned fibers and whiskers clearly suppress pullout by virtue of bending strains in the reinforcements that encourage fracture near the matrix crack plane. Indeed, fibers having low flexural resilience, such as SiC, tend to fail at the matrix crack plane when inclined to the crack,[67,68] whereas C fibers may still pullout over large distances.[69] Fiber alignment issues associated with pullout thus depend on fiber properties.

When fiber pullout does not contribute to toughness, as in many whisker-reinforced ceramics, the elastic energy and debonding energy terms tend to govern the fracture resistance, such that

$$\Delta\mathcal{G}_c \approx f d S^2/E + 4\Gamma_i f(d/R)/(1-f) \qquad (46)$$

To interpret this expression, it is essential to appreciate that the debond length d depends on the interface fracture energy Γ_i, misfit strain ε_{ii}^T, and friction coefficient. The associated relationships are unknown, but dimensional analysis suggests that[57,58]

$$d/R = H(E_f R(\varepsilon_{ii}^T)^2/\Gamma_i,\ S/E\varepsilon_{ii}^T,\ 1/\mu) \qquad (47)$$

where H is a function. The important point is that there remains much scope for controlling toughness by manipulating the interface debonding and sliding properties and by maximizing the fiber/whisker strength.

As already noted, resistance-curve effects cause the toughness to gradually build up to the asymptotic values. Consequently, the full toughness cannot usually be utilized. The toughening rate (tearing modulus) has not been broadly studied and trends are relatively unknown. However, some numerical results for pullout-dominated toughness indicate that asymptotic behavior is achieved only after considerable crack extension.[67]

(v) Ultimate Strength

When matrix cracking precedes ultimate failure, the *ultimate strength* coincides with fiber-bundle failure.[65] A simple estimate of this strength, based on weakest-link statistics that neglects interaction effects between failed fibers and ignores the stress supported by fractured fibers by means of stress transfer from the matrix through interface fraction, gives

$$\sigma_U = f\hat{S}\ \exp\left\{-\frac{[1-(1-\tau s/R\hat{S})^{m+1}]}{(m+1)[1-(1-\tau s/R\hat{S})^m]}\right\} \qquad (48)$$

with

$$(R\hat{S}/\tau s)^{m+1} = (A_0/2\pi R L_g)(RS_0/\tau s)^m \times [1-(1-\tau s/R\hat{S})^{m-1}]$$

where L_g is the specimen gauge length. The effect of the sliding stress on σ_U appears directly, as well as through its effect on the crack spacing s, while the effect of residual stress is present through its effect on τ. The ultimate strength is also expected to be influenced by the residual stress. Specifically, in systems for which the fiber is subject to residual compression, the axial compression should suppress fiber failure and elevate the ultimate strength to a level in excess of that predicted by Eq. (48). This effect may be estimated by regarding the matrix as clamping onto the fiber and, thus, simply superposing the residual stress onto $\hat{S}$.

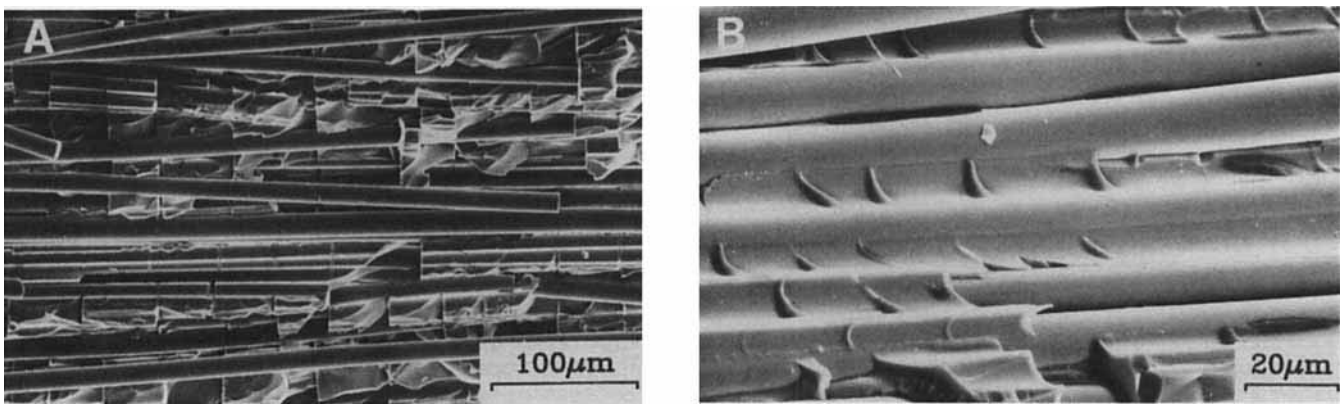

Fig. 33. Periodic matrix cracks formed upon loading above the steady-state matrix cracking stress.

(vi) Property Transition

Nonlinear macroscopic mechanical behavior on tension is most desirable for structural purposes. Analysis of the transition between this regime and the linear regime is important, and involves comparison of the basic trends in the steady-state matrix cracking stress, σ_0, and in the asymptotic fracture resistance, $\Delta\mathcal{G}_c$. Most significantly, σ_0 increases but $\Delta\mathcal{G}_c$ decreases as τ increases. These opposing trends with τ suggest the existence of an *optimum* τ that permits good matrix cracking resistance while still allowing high toughness. More specifically, a property transition is expected when the matrix cracking stress attains the stress needed for fiber-bundle failure. One estimate on the property transition can be obtained by simply allowing σ_0 to exceed the ultimate strength, σ_u, whereupon a nondimensional parameter β which governs the transition when τ is small is

$$\beta = \tau E \Gamma_m / S_0^3 R f \qquad (49)$$

Specifically, when β exceeds a critical value, brittle behavior initiates. This estimate has not been tested, and, furthermore, alternate parameters may be conceived.

(vii) Experimental Correlations

Uniaxially reinforced ceramic- and glass-matrix composites with either C or BN interlayer generally satisfy crack-front debonding requirements, and the materials exhibit axial and transverse mechanical properties that accord well with the above expressions for the matrix cracking stress and the ultimate strength.[62] To achieve these comparisons, each of the parameters in Eqs. (41) and (48) *has been independently ascertained*. As already mentioned, τ can be measured using various techniques: matrix crack spacing,[16,62] indentation push-through stress,[70,71] and matrix crack opening hysteresis.[61] The misfit strain ε_{ll}^T can also be determined using a variety of methods: X-ray or neutron line shifts, offset stresses in the crack opening, and residual displacements obtained from nanoindenter tests. Accurate values of the matrix fracture energy Γ_m and of the constituent elastic properties are also needed. Furthermore, it is noted that the comparison between theory and experiment for the matrix cracking stress is contingent upon having *accurate* values of the above parameters.

Correlations of trends in the ultimate strength are primarily contingent upon knowledge of the in situ mechanical properties of the fibers. Appreciation for these properties can be gained by examining and measuring fracture mirrors on the fiber fracture surfaces in the composite. Specifically, the distribution of mirror radii can be used to evaluate the axial stress S on the fiber of the fracture location.[72-74] Some typical results for two materials with different ultimate strength are shown in Fig. 35.[62] Limited experience has indicated that the ratio of median strengths scales with the ratio of composite ultimate strengths.

Based on the above experimental features that C and BN coatings are effective in terms of satisfying crack-front debonding and also providing a low sliding resistance, whereas amorphous oxides are incapable of debonding, it may be concluded that C and BN are the preferred coatings. However, both of these materials are susceptible to rapid oxidation[63-75] and mostly incapable of performing their required debonding and sliding functions at elevated temperatures in oxidizing environments. A variety of other coatings are thus under investigation. When such coatings have been developed, some of the more complex crack-opening and pullout constitutive laws presented may be needed to describe the mechanical properties of the composite.

(C) Bridging Grains

As already noted, bridging grains can be induced in two ways:[5,76] grain-boundary debonding and residual stress. Low fracture energy grain boundaries can allow debonding, as in whisker-reinforced materials, such that toughening involves the same terms described by Eq. (45). Indeed, a trend toward an increase in steady-state toughness is found in various polycrystalline Al_2O_3 materials as the grain-boundary fracture energy decreases.[77] Also, elongated grains, which allow larger debond lengths, could lead to higher toughness, as noted over a decade ago for both Si_3N_4[78] and Al_2O_3.[79] It is also known that, when the grain-boundary fracture energy is not low, as in sintered SiC, elongated grains do not lead to higher toughness. However, detailed application of Eq. (45) has not been attempted.

Residual stress-induced bridging occurs because circumferential compression causes the crack to circumvent local, highly stressed regions. Furthermore, it has been possible to rigorously demonstrate that such a bridging process increases the steady-state toughness in accordance with[37]

$$\Delta K_C = 2.5 f E \Delta\alpha \Delta T \sqrt{R} \qquad (50)$$

where f is the volume fraction of highly stressed grains that result in bridging ligaments and $2R$ the grain diameter. This increase in toughness arises because ligament failure occurs unstably and energy is dissipated in this process as acoustic waves, partly negated by some reduction in residual strain energy (c.f., the first two terms in Eq. (47)). For this process, elongated grains are not obviously beneficial.

(D) Multiple Mechanisms

The preceding sections have described microstructural issues concerned with toughness optimization when a single mechanism operates. In practice, more

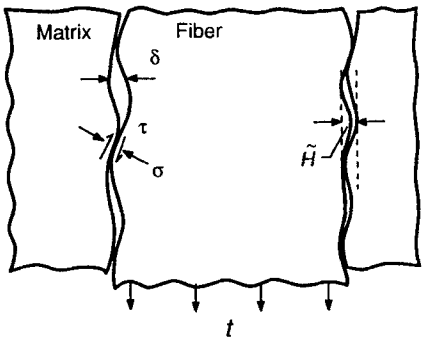

Fig. 34. Schematic of the pullout process for debonded fibers indicating the roles of fiber morphology, misfit strain, and friction coefficient.

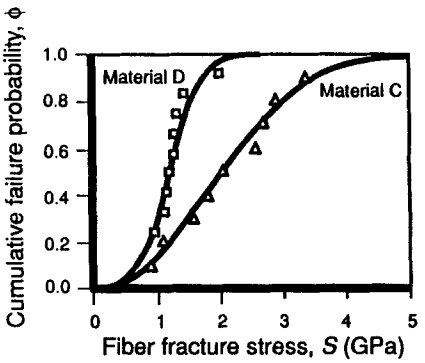

Fig. 35. Fiber strength distributions ascertained on two composites (refer to Fig. 32 for the corresponding stress–strain curves) using fracture mirror measurements.

than one mechanism may exist. Consequently, interactions between mechanisms must be considered. In some instances, the interactions may be highly *beneficial* and produce *synergism* between mechanisms. Such synergism has been illustrated to exist when both bridging and process-zone mechanisms operate simultaneously.[15] Conversely, some interaction effects can be *deleterious* and reduce the efficacy of the individual mechanisms.

Synergism is most likely when bridging and process-zone mechanisms interact. Multiplicative interactions are evident in this case because the crack surface tractions caused by bridging can expand the process-zone width h in the crack wake, causing an additional increase in shielding, proportional to this increase in h. Straightforward logic indicates that multiplicative toughening between bridging and process-zone effects should occur when the ratio of the bridging-zone size, L, to the process-zone width, h, is small, because bridging generates a new effective crack-tip toughness, that causes the process-zone size to further increase. Calculations of coupled bridging and process-zone effects have been performed in the case that the bridging tractions are constant (Dugdale zone). The results reveal two bounds given by[15]

$$K_c/K_m = \lambda_p \lambda_b \tag{51a}$$

the synergistic limit and

$$K_c/K_M = \sqrt{\lambda_p^2 + \lambda_b^2 - 1} \tag{51b}$$

the lower bound, where λ_p and λ_b are the toughening ratios for the process-zone and bridging mechanisms, respectively. Furthermore, and surprisingly, the synergistic limit was found to be obtained when $L/h \lesssim 10$. Rigorous experimental substantiation of synergism has yet to be obtained.

The interactions between either two bridging-zone mechanisms or two process-zone mechanisms are relatively unexplored. At the simplest level, two bridging mechanisms are additive with each $\Delta\mathcal{G}_c$ given by Eq. (3). However, the critical stretch u for one mechanism may be affected by the other, whereupon additivity may not be realized. Interactions between process-zone mechanisms are more difficult to express, because the zone sizes and the transformation strains are coupled. Preliminary attempts have been made to examine concurrent transformation and microcrack toughening which indicate that the coupling can result in an augmentation of toughness.

References

[1]F. F. Lange, "Powder Processing Science and Technology for Increased Reliability," *J. Am. Ceram. Soc.*, **72** [1] 3–15 (1989).

[2]R. W. Rice, Treatise On Materials Science and Technology, Vol. II; pp. 191–381. Academic Press, New York, 1978.

[3]A. G. Evans, "Structural Reliability: A Processing-Dependent Phenomenon," *J. Am. Ceram. Soc.*, **65** [3] 127–37 (1982).

[4]A. G. Evans, "New Opportunities in the Processing of High-Reliability Structural Ceramics"; pp. 989–1010 in Ceramic Transactions, Vol. 1, Ceramic Powder Science. Edited by G. L. Messing, E. R. Fuller, Jr., and H. Hausner. American Ceramic Society, Westerville, OH, 1989.

[5]R. F. Cook, B. R. Lawn, and C. J. Fairbanks, "Microstructure-Strength Properties in Ceramics: I, Effect of Crack Size on Toughness," *J. Am. Ceram. Soc*, **68** [11] 604–15 (1985).

[6]D. B. Marshall, "Strength Characteristics of Transformation-Toughened Zirconia," *J. Am. Ceram. Soc.*, **69** [3] 173–80 (1986).

[7]D. Shetty and J. Wang, "Crack Stability and Strength Distribution of Ceramics That Exhibit Rising Crack-Growth-Resistance [R-Curve] Behavior," *J. Am. Ceram. Soc.*, **72** [7] 1158–62 (1989).

[8]A. G. Evans and R. M. Cannon, "Toughening of Brittle Solids by Martensitic Transformations," *Acta Metall.*, **34** [5] 761–800 (1986).

[9]R. M. McMeeking and A. G. Evans, "Mechanics of Transformation-Toughening in Brittle Materials," *J. Am. Ceram. Soc.*, **65** [5] 242–47 (1982).

[10]B. Budiansky, J. W. Hutchinson, and J. C. Lambropolous, "Continuum Theory of Dilatant Transformation Toughening in Ceramics," *Int. J. Solids Struct.*, **19** [4] 337–55 (1983).

[11]D. B. Marshall, M. D. Drory, and A. G. Evans, "Transformation Toughening in Ceramics"; pp. 289–307 in Fracture Mechanics of Ceramics, Vol. 6. Edited by R. C. Bradt, A. G. Evans, F. F. Lange, and D. P. H. Hasselman. Plenum Press, New York, 1983.

[12]D. M. Stump and B. Budiansky, "Crack Growth Resistance in Transformation-Toughened Ceramics," *Int. J. Solids Struct.*, **25**, 635–46 (1989).

[13]B. Budiansky, J. C. Amazigo, and A. G. Evans, "Small-Scale Crack Bridging and the Fracture Toughness of Particulate-Reinforced Ceramics," *J. Mech. Phys. Solids*, **36** [2] 167–87 (1988).

[14]A. G. Evans and R. M. McMeeking, "On Toughening of Ceramics by Strong Reinforcements," *Acta Metall.*, **34**, 2435–41 (1986).

[15]J. C. Amazigo and B. Budiansky, "Interaction of Particulate and Transformation Toughening," *J. Mech. Phys. Solids*, **36**, 581–95 (1988).

Harvard University Report, MECH-112 (1989).

[16]J. Aveston, G. A. Cooper, and A. Kelly, "Single and Multiple Fracture"; pp. 15–26 in Conference Proceedings of the National Physical Laboratory: Properties of Fiber Composites. IPC Science and Technology Press, Surrey, England, 1971.

[17]B. Budiansky, J. W. Hutchinson, and A. G. Evans, "Matrix Fracture in Fiber-Reinforced Ceramics," *J. Mech. Phys. Solids*, **34**, 167–89 (1986).

[18]D. B. Marshall, B. N. Cox, and A. G. Evans, "The Mechanics of Matrix Cracking in Brittle-Matrix Fiber Composites," *Acta Metall.*, **33**, 2013–21 (1985).

[19]L. N. McCartney, "Mechanics of Matrix Cracking in Brittle-Matrix Fiber-Reinforced Composites," *Proc. R. Soc. London, Series A–Mathematical and Physical Sciences*, **409** [1837] 329–50 (1987).

[20]M. V. Swain and L. R. F. Rose, "Strength Limitations of Transformation-Toughened Zirconia Alloys," *J. Am. Ceram. Soc.*, **69** [7] 511–18 (1986).

[21]A. G. Evans, N. H. Burlingame, W. M. Kriven, and M. D. Drory, "Martensitic Transformations in Zirconia Particle Size Effects and Toughening," *Acta Metall.*, **29**, 447–56 (1981).

[22]R. Dauskhardt, D. K. Veirs, and R. O. Ritchie, "Spatially Resolved Raman Spectroscopy Study of Transformed Zones in Magnesia-Partially-Stabilized Zirconia," *J. Am. Ceram. Soc.*, **72** [7] 1124–30 (1989).

[23]I. W. Chen and P. E. Reyes-Morel, "Implications

of Transformation Plasticity in ZrO_2-Containing Ceramics: I, Shear and Dilitation Effects," *J. Am. Ceram. Soc.*, **69** [3] 181–89 (1986).

[24]L. R. F. Rose, "Kinematical Model for Stress-Induced Transformation around Cracks," *J. Am. Ceram. Soc.*, **69** [3] 208–12 (1986).

[25]M. Rühle, N. Claussen, and A. H. Heuer, "Transformation and Microcrack Toughening as Complementary Processes in ZrO_2-Toughened Al_2O_3," *J. Am. Ceram. Soc.*, **69** [3] 195–97 (1986).

[26]D. J. Green, R. H. J. Hannink, and M. V. Swain, Transformation Toughening of Ceramics; pp. 1–91. CRC Press, Inc., Boca Raton, FL, 1989.

[27]F. E. Buresch, "A Structure Sensitive K_{Ic}-Value and Its Dependence on Grain Size Distribution, Density and Microcrack Interaction"; pp. 835–47 in Fracture Mechanics of Ceramics, Vol. 4. Edited by R. C. Bradt, D. P. H. Hasselman, and F. F. Lange. Plenum, New York, 1975.

[28]R. G. Hoagland, A. P. Rosenfield, and G. T. Hahn, *Metall. Trans.*, **3**, 123 (1972).

[29]R. G. Hoagland, J. D. Embury, and D. J. Green, "On the Density of Microcracks Formed During the Fracture of Ceramics," *Scr. Metall.*, **9** [9] 907–909 (1975).

[30]A. G. Evans, "On the Formation of a Crack Tip Microcrack Zone," *Scr. Metall.*, **10**, 93 (1976).

[31]M. Rühle, A. G. Evans, R. M. McMeeking, P. G. Charalambides, and J. W. Hutchinson, "Microcrack Toughening in Alumina/Zirconia," *Acta Metall.*, **35** [11] 2701–10 (1987).

[32]K. T. Faber, "Microcrack Toughening in SiC/TiB_2"; unpublished work.

[33]A. G. Evans and K. T. Faber, "Crack-Growth Resistance of Microcracking Brittle Materials," *J. Am. Ceram. Soc.*, **67** [4] 255–60 (1984).

[34]J. W. Hutchinson, "Crack Tip Shielding by Microcracking in Brittle Solids," *Acta Metall.*, **35** [7] 1605–19 (1987).

[35]A. Quinten and V. Arnold, "Observation of Stable Crack Growth Using a Scanning Acoustic Microscope"; to be published in *Mater. Sci. Eng.*

[36]B. Budiansky and R. J. O'Connell, "Elastic Moduli of a Cracked Solid," *Int. J. Solids Struct.*, **12** [2] 81–97 (1976).

[37](a) W. Shum, "Bridging Effects on Toughness"; Ph.D. Thesis. Harvard University, Cambridge, MA, (1989). (b) W. Shum and J. W. Hutchinson; unpublished work.

[38]J. R. Rice, Harvard University Report, MECH-116 (1989).

[39]V. D. Krstic, *Philos. Mag.*, **A48**, 695 (1983).

[40]M. F. Ashby, F. J. Blunt, and M. Bannister, "Flow Characteristics of Highly Constrained Metal Wires," *Acta Metall.*, **37** [7] 1847–57 (1989).

[41]L. S. Sigl, P. Mataga, B. J. Dalgleish, R. M. McMeeking, and A. G. Evans, "On the Toughness of Brittle Materials Reinforced with a Ductile Phase," *Acta Metall.*, **36** [3] 517–22 (1988).

[42]D. B. Marshall, M. Shaw, A. H. Heuer, M. Readey, R. O. Ritchie, and R. H. Dauskardt; unpublished work.

[43]P. Hing and G. W. Groves, "The Strength and Fracture Toughness of Polycrystalline Magnesium Oxide Containing Metallic Particles and Fibres," *J. Mater. Sci.*, **7** [4] 427–34 (1972).

[44]G. A. Cooper and A. Kelly, "Tensile Properties of Fiber-Reinforced Metals—Fracture Mechanics," *J. Mech. Phys. Solids*, **15** [4] 279–94 (1967).

[45]W. W. Gerberich, *J. Mech. Phys. Solids*, **19**, 71 (1971).

[46]C. K. Elliott, G. R. Odette, G. E. Lucas, and J. W. Sheckard, "Toughening Mechanisms in Intermetallic γ-TiAl Alloys Containing Ductile Phases," *Mater. Res. Soc. Proc.*, **120**, 95–102 (1988).

[47]H. C. Cao, B. J. Dalgleish, H. E. Dève, C. K. Elliott, A. G. Evans, R. Mehrabian, and G. R. Odette, "A Test Procedure for Characterizing the Toughening of Brittle Intermetallics by Ductile Reinforcements," *Acta Metall.*, **37** [11] 2969–77 (1989).

[48]W. W. Gerberich and E. Kurman, "New Contributions to the Effective Surface-Energy Cleavage," *Scr. Metall.*, **19** [3] 295–98 (1985).

[49]M. S. Newkirk, A. W. Urqhart, and H. R. Zwicker, *J. Mater. Res.*, **1**, 81 (1986).

[50]B. Flinn, M. Rühle, and A. G. Evans, "Toughening in Composites of Al_2O_3 Reinforced with Al," *Acta Metall.*, **37** [11] 3001–3002 (1989).

[51]V. K. Sarin (ed.), "Science of Hard Materials-3," *Mater. Sci. Eng.*, **A105/106**, 5–21 (1988).

[52]B. Budiansky and J. C. Amazigo, "Toughening by Aligned, Frictionally Constrained Fibers," *J. Mech. Phys. Solids*, **37** [1] 93–109 (1989).

[53](a) L. R. F. Rose, "Crack Reinforcement by Distributed Springs," *J. Mech. Phys. Solids*, **35** [4] 383–405 (1987). (b) P. Mataga, "Toughening by Ductile Particles"; to be published in *Acta Metall.*

[54]L. S. Sigl and E. Exner, "Experimental Study of the Mechanics of Fracture in WC-Co Alloys," *Metall. Trans. A*, **18**, 1299–308 (1987).

[55]L. S. Sigl and H. F. Fischmeister, "On the Fracture-Toughness of Cemented Carbides," *Acta Metall.*, **36** [4] 887–97 (1988).

[56]M. He and J. W. Hutchinson, "Kinking of a Crackout of an Interface," *J. Appl. Mech.*, **56**, 270–78 (1989).

[57]P. G. Charalambides and A. G. Evans, "Debonding Properties of Residually Stressed Brittle-Matrix Composites," *J. Am. Ceram. Soc.*, **72** [5] 746–53 (1989).

[58]L. S. Sigl and A. G. Evans, "Effects of Residual Stress and Frictional Sliding on Cracking and Pull-Out in Brittle Matrix Composites," *Mech. Mater.*, **8**, 1–12 (1989).

[59]M. D. Thouless and A. G. Evans, "Effect of Pull-Out on the Mechanical Properties of Brittle Matrix Composites," *Acta Metall.*, **36** [3] 517–22 (1988).

[60]K. M. Prewo and J. J. Brennan, "Silicon Carbide-Fiber-Reinforced Glass-Ceramic-Matrix Composites Exhibiting High Strength and Toughness," *J. Mater. Sci.*, **17**, 1201–206 (1982).

[61]D. B. Marshall and A. G. Evans, "Failure Mechanisms in Ceramic-Fiber/Ceramic-Matrix Composites," *J. Am. Ceram. Soc.*, **68** [5] 225–31 (1985).

[62]H. C. Cao, E. Bischoff, M. Rühle, A. G. Evans, D. B. Marshall, J. J. Brennan, and O. Sbaizero, "The Effect of Interfaces on the Mechanical Performance of Fiber-Reinforced Brittle Materials"; to be published in *J. Am. Ceram. Soc.*

[63](a) D. C. Phillips, "The Fracture Energy of Carbon-Fibre-Reinforced Glass," *J. Mater. Sci.*, **7** [10] 1175–91 (1972). (b) E. Bischoff, O. Sbaizero, M. Rühle, and A. G. Evans, "Microstructural Studies of the Interfacial Zone of a SiC-Fiber-Reinforced Lithium Aluminum Silicate Glass-Ceramic," *J. Am. Ceram. Soc.*, **72** [5] 741–45 (1989).

[64]H. L. Oh and I. Finnie, *Int. J. Fract. Mech.*, **6**, 287 (1970).

[65]M. D. Thouless, O. Sbaizero, L. S. Sigl, and A. G. Evans, "Effect of Interface Mechanical Properties on Pullout in SiC-Fiber-Reinforced Lithium Aluminum Silicate Glass-Ceramic," *J. Am. Ceram. Soc.*, **72** [4] 525–32 (1989).

[66]G. H. Campbell, B. J. Dalgleish, M. Rühle, and A. G. Evans, "Whisker Toughening: A Comparison between Al_2O_3 and Si_3N_4 Toughened with SiC"; to be published in *J. Am. Ceram. Soc.*

[67]C. L. Hom, O. Sbaizero, and A. G. Evans, "Resistance Curves in Fiber-Toughened Ceramics"; unpublished work.

[68]M. Rühle, B. J. Dalgleish, and A. G. Evans, "On the Toughening of Ceramics by Whiskers," *Scr. Metall.*, **21**, 681–86 (1987).

[69]K. M. Prewo, "Tension and Flexural Strength of Silicon Carbide Fibre-Reinforced Glass Ceramics," *J. Mater. Sci.*, **21** [10] 3590–600 (1986).

[70]D. B. Marshall and W. Oliver, "Measurement of Interfacial Mechanical Properties in Fiber-Reinforced Ceramic Composites," *J. Am. Ceram. Soc.*, **70** [8] 542–48 (1987).

[71]T. P. Wiehs, C. M. Dick, and W. D. Nix, "The Frictional Resistance to Sliding of a SiC Fiber in a Brittle Matrix," *Mater. Res. Soc. Symp. Proc.*, **120**, 247–52 (1989).

[72]J. J. Mecholsky and S. R. Powell (eds.), Fractography of Ceramic and Metal Failures, STP 827; pp. 187–95. American Society for Testing and Materials, Philadelphia, PA, 1984.

[73]J. F. Jamet, D. Lewis, and E. Y. Luh, "Characterization of Mechanical Behavior and Fractographic Observations on Compglas SiC/LAS Composites," *Ceram. Eng. Sci. Proc.*, **5** [7–8] 625–42 (1984).

[74]A. J. Eckel and R. C. Bradt, "Strength Distribution of Reinforcing Fibers in a Nicalon Fiber/Chemically Vapor Infiltrated Silicon Carbide Matrix Composite," *J. Am. Ceram. Soc.*, **72** [3] 455–58 (1989).

[75]E. Y. Luh and A. G. Evans, "High-Temperature Mechanical Properties of a Ceramic Matrix Composite," *J. Am. Ceram. Soc.*, **79** [7] 466–69 (1987).

[76]B. R. Lawn, "Physics of Fracture," *J. Am. Ceram. Soc.*, **66** [2] 83–91 (1983).

[77]R. F. Cook, "Segregation Effects on the Fracture of Brittle Materials"; to be published in *Acta Metall.*

[78]F. F. Lange, "Fracture Toughness of Si_3N_4 as a Function of Initial α-Phase Content," *J. Am. Ceram. Soc.*, **62** 428 (1979).

[79]A. G. Evans, A. H. Heuer, and D. L. Porter, "The Fracture Toughness of Ceramics"; pp. 529–56 in Fracture 77, Advances in Research on the Strength and Fracture of Materials, Fourth International Conference on Fracture, Vol. 1. Edited by D. M. R. Taplin. Pergamon, New York, 1978.

□